Appendix A

A Second Interaction Region For Gamma-Gamma and Gamma-Electron collisions

R. Brinkmann[1], I. Ginzburg[2], N. Holtkamp[1], G. Jikia[3], O. Napoly[4], E. Saldin[5], E. Schneidmiller[5], V. Serbo[6], G. Silvestrov[7], V. Telnov[7] (Editor), A. Undrus[7], M. Yurkov[8]

1) DESY,
2) Inst. of Mathematics, Novosibirsk,
3) Alexander von Humboldt Fellow, Uni Freiburg and IHEP, Protvino,
4) Saclay,
5) Automatic Syst. Corp, Samara,
6) Novosibirsk State University,
7) Inst. of Nucl. Physics, Novosibirsk,
8) JINR, Dubna

Contents

A.1 Introduction

Linear colliders offer unique opportunities to study $\gamma\gamma$, γe interactions. Using the laser backscattering method one can obtain $\gamma\gamma$ and γe colliding beams with an energy and luminosity comparable to that in e^+e^- collisions. This can be done with relatively small incremental cost. The expected physics in these collisions (see section 2) is very rich and complementary to that in e^+e^- collisions. Some characteristic examples are:

- a $\gamma\gamma$ collider provides unique opportunities to measure the two-photon decay width of the Higgs boson, and to search for relatively heavy Higgs states in the extended Higgs models such as MSSM;
- a $\gamma\gamma$ collider is an outstanding W factory, with a WW pair production cross section by a factor of 10–20 larger than in e^+e^- and with a potential of producing $10^6 - 10^7$ W's per year, allowing a precision study of the anomalous gauge boson interactions;
- a $\gamma\gamma$, γe collider is a remarkable tool for searching for new charged particles, such as supersymmetric particles, leptoquarks, excited states of electrons, etc., as in $\gamma\gamma$, γe collisions they are produced with cross sections larger than in e^+e^- collisions;
- at a γe collider charged supersymmetric particles with masses higher than the beam energy could be produced as well as the structure of the photon could be measured with comparable presision to studies of the proton at HERA..

In order to make this new field of particle physics accessible it would be wise to have at the TESLA (SBLC) two interaction regions (IR): one for e^+e^- collisions and the other for $\gamma\gamma$, γe collisions. In this appendix we will describe physics at photon colliders, expected $\gamma\gamma$, γe luminosities, and the design of the interaction region required for $\gamma\gamma$, γe collisions.

The general scheme of a photon collider is shown in Fig. A.1. Two electron beams after the final focus system are traveling toward the interaction point (IP). At a distance of order 1 cm upstream from the IP, referred to hereafter as the conversion point (CP), the laser beam is focused and Compton backscattered by the electrons, resulting in the high energy beam of photons. With reasonable laser parameters one can "convert" most of electrons to high energy photons. The photon beam follows the original electron direction of motion with a small angular spread of order $1/\gamma$, arriving at the IP in a tight focus, where it collides with a similar opposing high energy photon beam or with an electron beam. The photon spot size at the IP may be almost equal to that of electrons at IP and therefore the luminosity of $\gamma\gamma$, γe collisions will be of the same order as the "geometric" luminosity of basic ee beams (positrons are not necessary for a photon collider).

After multiple Compton scattering the electrons have a wide energy spread $E = (0.02 - 1)E_0$, and either follow to the IP or are swept aside by a small pulsed magnet with $B \sim 1$ T. With the deflecting magnet one can get better quality of colliding beams,

smaller background and disruption angles. The removal of the disrupted electron beams is a challenging problem and can be solved in simplest way in the crab crossing scheme of beam collisions.

The effects limiting the luminosity of $\gamma\gamma$ collisions are different from those in e^+e^- collisions; the beamstrahlung and instabilities are absent and only the coherent e^+e^- pair production in the field of oppositely moving "used"(spent) electron beam is still important. Therefore the electron beams for $\gamma\gamma$ collisions may have the smaller horizontal size at the IP than in e^+e^- case, and consequently the larger luminosity is attainable. To reach ultimate luminosity in $\gamma\gamma$ collisions, the beams with smaller horizontal emittance are required, which demands reoptimization of the damping rings or use of low emittance RF guns. The latter opportunity seems promising.

The laser required for conversion must be in μm wave length region, with few Joules flash energy, about one picosecond duration and $20 - 30$ kW average power. Such a laser can be a solid state laser with diode pumping and chirped pulse amplification. These parameters can be obtained also with a one pass free-electron laser. For 1–2 TeV c.m.s. energy collider, the optimum wave length is 2–4 μm and here FEL is the only choice. The optical mirror system in tight space inside the detector which transports the laser beam into the conversion points is also a challenging task.

The idea of producing γe and $\gamma\gamma$ collisions at linear colliders via Compton backscattering has been proposed and studied by scientists from Novosibirsk [1]–[5]. Photon colliders were considered also in [6]–[28]. A review of $\gamma\gamma$, γe colliders, physics opportunities and available technologies can be found in the proceedings of a workshop on gamma-gamma colliders held at Berkeley [30] and in the Zero Design Report of NLC[31].

The physics program at photon colliders was discussed at Workshops on Physics at Linear Colliders (Saariselka,1991; Waikoloa,1993, Morioka-Appi,1995) at Workshops on $\gamma\gamma$ Collisions (San Diego, 1992; Sheffield, 1995), in reviews [32]–[38] and in numerous papers.

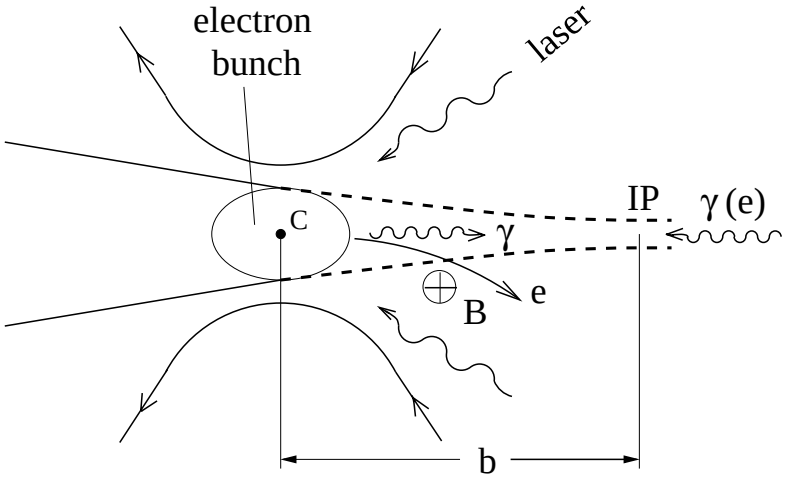

Figure A.1: *Scheme of a $\gamma\gamma$; γe collider.*

A.2 Physics at $\gamma\gamma$, γe collider

A.2.1 Introduction

In what follows we assume the following parameters of $\gamma\gamma$ and γe collisions (we use abbreviation PLC – Photon Linear Collider – for these modes). Here $W_{\gamma\gamma}$ and $W_{\gamma e}$ denote c.m.s. energies of $\gamma\gamma$ or γe systems, respectively.

- One can vary both initial electron energy and laser frequency[1] to have the most sharp possible spectrum of photons with a peak at the necessary energy. High energy photons will have high degree of longitudinal polarization.
- The width of the high energy luminosity peak will be $\Delta W_{\gamma\gamma}/W_{\gamma\gamma} \approx 0.15$, $\Delta W_{\gamma e}/W_{\gamma e} \approx 0.05$ [2].
- The annual (10^7 s) $\gamma\gamma$ luminosity will be about 10–30 fb^{-1} (in the high energy peak) with possible upgrade of luminosity by one order of magnitude (sect.4.5.3).

- The annual γe luminosity will be about 15–50 fb^{-1} with about 5% monochromaticity.

A.2.2 Higgs boson physics

Discovery and study of Higgs boson(s) properties will be of primary importance at future pp and linear e^+e^- and $\gamma\gamma$ colliders. The survey of the Higgs physics opportunities of PLC is simultaneously a very good example showing how the complete phenomenological portrait is obtained only by combining the complementary information available from these distinct types of machines.

Measurements of the Higgs boson couplings.

Using the $\gamma\gamma$ collider mode a unique possibility appears [48, 14, 49, 50, 15, 51] to produce the Higgs boson as an s-channel resonance decaying, for instance, into $b\bar{b}$:

$$\gamma\gamma \to h^0 \to b\bar{b}.$$

Assuming that 300-500 GeV linear collider will first start operating in e^+e^- mode, the mass of the h^0 will already be known from the Bjorken reaction $e^+e^- \to Z^* \to Zh$, and we can tune the energy of the $\gamma\gamma$ collider so that the photon-photon luminosity spectrum peaks at m_h. The cross section at PLC is proportional to the product $\Gamma(h \to \gamma\gamma) \cdot BR(h \to b\bar{b})$. The Higgs two-photon decay width is of special interest since it appears at the one-loop level. Thus, any heavy charged particles which obtain their masses from electroweak symmetry breaking can contribute in the loop. The branching ratio $BR(h \to b\bar{b})$ will also already be known from e^+e^- annihilation. Indeed,

[1] The Free Electron Laser seems preferable for this goal.

[2] Outside the high energy peak, usually there is a flat part of the luminosity distribution with 2–10 times larger total luminosity depending on the details of the collision scheme (see sect.4).

measuring $\sigma(ZH)$ (in the missing mass mode) and $\sigma(ZH)BR(h \to b\bar{b})$ in e^+e^- mode of the linear collider we can compute

$$BR(h \to b\bar{b}) = \frac{[\sigma(ZH)BR(h \to b\bar{b})]}{\sigma(ZH)},$$

the error in the branching ratio is estimated at $\pm(8 \div 10)\%$ [52].

Then measuring the rate for the Higgs boson production in $\gamma\gamma$ mode of the linear collider (accuracy $\pm 5\%$) we can determine the value of the Higgs two-photon width itself (accuracy $\pm(11 \div 13)\%$) [52]

$$\Gamma(h \to \gamma\gamma) = \frac{[\Gamma(h \to \gamma\gamma)BR(h \to b\bar{b})]}{BR(h \to b\bar{b})}.$$

The main background to the h^0 production is the continuum production of $b\bar{b}$ and $c\bar{c}$ pairs. In this respect, the availability of high degree of photon beams circular polarization is crucial, since for the equal photon helicities ($\pm\pm$) that produce spin-zero resonant states, the $q\bar{q}$ QED Born cross section is suppressed by the factor m_q^2/s [14]. Another potentially dangerous backgrounds originate from the resolved-photon processes [54, 55, 56] in which a gluon from the photon structure function produces $b\bar{b}$, $c\bar{c}$ pairs, and from the continuum production of $b\bar{b}$ pairs accompanied by the radiation of additional gluon [57], calculated taking into account large QCD $\mathcal{O}(\alpha_s)$ radiative corrections [56], which are not suppressed even for the equal photon helicities. However, these detailed studies have shown that the Higgs signal can still be observed well above the background with the statistical error of the Higgs cross section at the 6-10% level with 20 fb^{-1} in the wide range of Higgs mass $60 \div 150$ GeV. As the width $\Gamma(h \to \gamma\gamma)$ computed in the presence of an extra generation with $m_L = 300$ GeV and $m_U = m_D = 500$ GeV drops to 15-30% of its SM value [49] this accuracy is sufficient to exclude the contribution of a heavy fourth generation at the 5σ level.

If the Higgs boson is in the intermediate mass range, as it is implied by the MSSM, it is also most likely to be observed at the LHC in the gluon fusion reaction in its $\gamma\gamma$ decay mode $gg \to h^0 \to \gamma\gamma$, so that the measured rate is proportional to $BR(h \to gg)\cdot\Gamma(h \to \gamma\gamma)$ (with an error of order $\pm 22\%$ at $m_{h_{SM}} = 120$ GeV [58]). The observable cross section for the $\gamma\gamma$ signal at the LHC can depend quite strongly on the masses and couplings of the superpartners and Higgs bosons, particularly if they are not too heavy, and it varies from a few fb to more than 100 fb over the parameter space of the MSSM, even in the scenario that supersymmetry is not discovered at LEP2 [59]. In general, interpretation of this one number is ambiguous, however by combining this number with the value of the Higgs two-photon decay width, measured in $\gamma\gamma$ and e^+e^- experiments one can calculate the two-gluon branching ratio $BR(h \to gg)$. Moreover, by measuring in $e^+e^- \to Zh$, $e^+e^- \to \nu_e\bar{\nu}_e h$ (W^+W^--fusion) reactions the event rates for $h \to \gamma\gamma$ and $h \to b\bar{b}$, one can compute the two-photon branching ratio

$$\begin{aligned} BR(h \to \gamma\gamma) &= BR(h \to b\bar{b})\frac{[\sigma(Zh)BR(h \to \gamma\gamma)]}{[\sigma(Zh)BR(h \to b\bar{b})]} \\ &= BR(h \to b\bar{b})\frac{[\sigma(\nu_e\bar{\nu}_e h)BR(h \to \gamma\gamma)]}{[\sigma(\nu_e\bar{\nu}_e h)BR(h \to b\bar{b})]} \end{aligned}$$

with the accuracy $\pm(20 \div 30)\%$ [52] and, finally, compute in a model-independent way the total and partial Higgs decay widths that are directly related to fundamental couplings

$$\Gamma_h^{tot} = \frac{\Gamma(h \to \gamma\gamma)}{BR(h \to \gamma\gamma)},\ \Gamma(h \to b\bar{b}) = \Gamma_h^{tot} BR(h \to b\bar{b}),\ \Gamma(h \to gg) = \Gamma_h^{tot} BR(h \to gg).$$

For the Higgs bosons heavier than $2M_Z$ the Higgs signal in $\gamma\gamma$ collisions can be observed in ZZ decay mode [49, 53] if one of the Z's is required to decay to l^+l^- to suppress the huge tree-level $\gamma\gamma \to W^+W^-$ continuum background. However, even though there is no tree-level ZZ continuum background, such a background due to the reaction $\gamma\gamma \to ZZ$ does arise at the one-loop level in the electroweak theory [60, 61, 62] which makes the Higgs observation in the ZZ mode impossible for $m_h > (350 \div 400)$ GeV. It was found that for $185 < m_h < 300$ GeV the ZZ mode will provide a 8-11% determination of the quantity $\Gamma(h \to \gamma\gamma) \cdot BR(h \to ZZ)$.

In the 150-185 GeV window, the W^+W^- and $b\bar{b}$ Higgs decay modes are comparable. A recent study [63] has looked at the W^+W^--channel by also taking into account the interference between the $\gamma\gamma \to W^+W^-$ continuum and the s-channel Higgs exchange, which are all of the same electroweak order on resonance. Unfortunately, for the measurement of the interference pattern in this reaction the energy resolution less than 1 GeV is required that is practically impossible to reach at photon colliders. So, the accuracy of the two-photon Higgs width measurement might not be better than 20-25% in this region.

If $M_H \sim 2M_t$, the interference between QED process $\gamma\gamma \to t\bar{t}$ and resonant one $\gamma\gamma \to H \to t\bar{t}$ can be used to obtain the value of Higgs coupling with t–quark [64].

Because of the dominance of the W loop contribution in the three family case, the $h\gamma\gamma$ vertex is also very sensitive to any **anomalous couplings of the Higgs or W bosons** hW^+W^-, $W^+W^-\gamma$, $h\gamma\gamma$ [65, 43, 66]. The sensitivity to anomalies in these couplings can be comparable to that provided by LEP2 data.

The anomalous $Z\gamma H$ interactions can be studied via $e\gamma \to eH$ process with longitudinally polarized electrons [67].

Finally, the production of Higgs bosons at a $\gamma\gamma$ collider offers a special experimental opportunity to determine the CP properties of a particular Higgs boson [68, 69, 70]. If $\vec{E}$ and $\vec{B}$ are electric and magnetic field strengths, a CP-even Higgs boson H^0 couples to the combination $\vec{E}^2 - \vec{B}^2$, while a CP-odd Higgs boson A^0 couples to $\vec{E}\vec{B}$. The first of these structures couples to linearly polarized photons with the maximal strength if the polarizations are parallel, the letter if the polarizations are perpendicular:

$$\sigma \propto (1 \pm l_{\gamma 1} l_{\gamma 2} \cos 2\phi),$$

where $l_{\gamma i}$ are the degrees of linear polarization and ϕ is the angle between $\vec{l}_{\gamma 1}$ and $\vec{l}_{\gamma 2}$. The $\pm$ sign corresponds to $CP = \pm 1$ scalar particle. The attainable degree of linear polarization l_γ at PLC depends on the value of $z_m = (W_{\gamma\gamma})_{max}/2E_0$ which can be changed in the case of free electron laser. For $z_m = 0.82$ the degree of linear polarization is $l_\gamma \sim 0.33$ only, but $l_\gamma \geq 0.8$ at $z_m \leq 0.5$ that is sufficient to study the CP quantum numbers of Higgs with $m_H \leq 250$ GeV at $2E_0 = 500$ GeV ee collider.

Moreover, if the Higgs boson is a mixture of CP-even and CP-odd states, as can occur *e.g.* in two-doublet Higgs models with CP-violating neutral sector [71], the interference of these two terms gives rise to a CP-violating asymmetry in the total rate for Higgs boson production for $(++)$ and $(--)$ helicities of the initial photons [68]

$$\mathcal{A} = \frac{\sigma_{++}(\gamma\gamma \to H) - \sigma_{--}(\gamma\gamma \to H)}{\sigma_{++}(\gamma\gamma \to H) + \sigma_{--}(\gamma\gamma \to H)}.$$

Experimentally the measurement of the asymmetry is achieved by simultaneously flipping the helicities of both of the initiating laser beams. One finds [68] that the asymmetry is typically larger than 10% and is observable for a large range of two-doublet parameter space if CP violation is present in the Higgs potential.

The discovery of the Higgs boson.

In principle it might be possible to detect the Higgs boson at PLC for m_H somewhat nearer to $\sqrt{s_{ee}}$ than the $0.7\sqrt{s_{ee}}$ that appears to be feasible via direct e^+e^- collisions [72], as the full $\gamma\gamma$ c.m.s. energy $W_{\gamma\gamma}$ converts into the Higgs resonance, and the parameters of the initial electron and laser beams can be configured so that the photon spectrum peaks slightly above $W_{\gamma\gamma} = 0.8\sqrt{s_{ee}}$. However, for $\sqrt{s_{ee}} = 500$ GeV the detection of the SM Higgs boson in the range of greatest interest, which cannot be accessed by direct e^+e^- collisions, *i.e.* $m_H \geq 350$ GeV, is problematic because of the large one-loop ZZ background [60, 61, 62] discussed above.

The PLC potential to discover Higgs bosons is especially attractive in the search for heavy Higgs states in the extended models such as MSSM [49, 72]. The most important limitation of a e^+e^- collider in detecting the MSSM Higgs bosons is the fact that they are produced only in pairs, H^0A^0 or H^+H^-, and the parameter range for which the production process $Z^* \to H^0A^0$ has adequate event rate is limited by the machine energy to $m_{A^0} \sim m_{H^0} \leq \sqrt{s_{ee}}/2 - 20$ GeV ($m_{H^0} \sim m_{A^0}$ for large m_{A^0}) [72]. At $\sqrt{s_{ee}} = 500$ GeV, this means $m_{A^0} \leq 230$ GeV. As $e^+e^- \to H^+H^-$ is also limited to $m_{H^\pm} \sim m_{A^0} \leq (220 \div 230)$ GeV, it could happen that only a rather SM-like h^0 is detected in e^+e^- mode of the linear collider, and none of the other Higgs bosons are observed. On the other hand, H^0 and A^0 can be singly produced as s-channel resonances in the $\gamma\gamma$ mode and PLC might allow the discovery of the H^0 and/or A^0 up to higher masses [49, 72]. Particularly interesting decay channels at moderate $\tan\beta$ and below $t\bar{t}$ threshold are $H^0 \to h^0h^0$ (leading to a final state containing four b quarks) and $A^0 \to Zh^0$. These channels are virtually background free unless $m_h^0 \sim m_W$, in which case the large $\gamma\gamma \to W^+W^-$ continuum background would have to be eliminated by b-tagging. Discovery of the A^0 or H^0 up to about $0.8\sqrt{s_{ee}}$ would be possible. For large $\tan\beta$, the detection of the A^0 or H^0 in the $b\bar{b}$ channel should be possible for masses $\leq 0.8\sqrt{s_{ee}}$ [49, 72], provided that effective luminosities as high as 200 fb^{-1} can be accumulated (Sect. 4.5.3).

A.2.3 Gauge boson physics

Without the discovery of a Higgs boson at LEP2, LHC or linear collider, the best alternative to study the symmetry breaking sector lies in the study of the self-couplings

of the W. The PLC will be the dominant source of the W^+W^- pairs at future linear colliders due to the reaction $\gamma\gamma \to \mathrm{W^+W^-}$ with the large cross section, that fast reaches at high energies its asymptotic value $\sigma_W = 8\pi\alpha^2/M_W^2 \approx 81$ pb [74], which is at least an order of magnitude larger than the cross section of W^+W^- production in e^+e^- collisions. With the rate of about 1–3 million of W pairs per year PLC can be really considered as **a W factory** and an ideal place to conduct precision tests on the anomalous triple [75, 34] and quartic [76, 34, 77] couplings of the W bosons. In conjunction with $e^+e^- \to W^+W^-$ one can reach much better precision on these couplings. In addition, in the process of triple WWZ vector boson production it is possible to probe the tri-linear ZWW and quartic couplings [77, 78, 34, 79] as well as the C violating anomalous ZWW, γZWW interactions [79]. With the natural order of magnitude on anomalous couplings [80], one needs to know the SM cross sections with a precision better than 1% to extract these small numbers. The predictions for W pair production, including full electroweak radiative corrections in the SM are known with very little theoretical uncertainty at least for energies below 1 TeV [81, 82].

The process of W production with the highest cross section in γe collisions, $\gamma e \to \mathrm{W}\nu$, with the asymptotic cross section of $\sigma_{\gamma e \to \mathrm{W}\nu} = \sigma_W / 8\sin^2\Theta_W \approx 43$ pb [74], is very sensitive to the admixture of right–handed currents in W coupling with fermions, as $\sigma_{\gamma e \to \mathrm{W}\nu} \propto (1 - 2\lambda_e)$. This process was studied in details in refs. [83], where the radiative corrections were taken into account.

The list of main processes with the W and Z production at PLC within SM can be found in refs. [84, 85], see Fig. A.2. When the energy increases, the cross sections of a number of **higher–order processes** become large enough. The catalogue of such processes of third order in SM is given in ref. [86]. It is will even be possible to study at PLC pure one-loop induced SM reactions like elastic light-by-light scattering $\gamma\gamma \to \gamma\gamma$ [87], γZ [88] or ZZ [60, 61, 62] pair production processes, all of which are dominated by the W loop contribution at high energies.

At higher energy the effective W luminosity becomes substantial enough to allow for the study of $W^+W^- \to W^+W^-$, ZZ **scattering** in the reactions $\gamma\gamma \to WWWW$, $WWZZ$, when each incoming photon turns into a virtual WW pair, followed by the scattering of one W from each such pair to form WW or ZZ [34, 33, 89, 90]. The result is that a signal of SM Higgs boson with m_H up to 700 GeV (1 TeV) could be probed in these processes at 1.5 TeV (2 TeV) PLC, assuming integrated luminosity of 200 fb^{-1} (300 fb^{-1}). The $\gamma Z \to WW$ **scattering** can be studied in the $\gamma e \to \mathrm{W^+W^-}e$ reaction with the cross section of about 5 pb at $W_{\gamma e} \approx 0.4$ TeV and 27 pb at $W_{\gamma e} \approx 2$ TeV [91, 92].

A.2.4 Physics of t–quarks

The threshold effects will be investigated at PLC mode [93, 94] similar to those at e^+e^- mode [95]. The strong dependence on photon helicities provides opportunity to see delicate details of $t\bar{t}$ interaction near the threshold, thought the broader momentum spread of the photon beams do not allow to measure the exitation curve with the same precision as in $\mathrm{e^+e^-}$ energy scan.

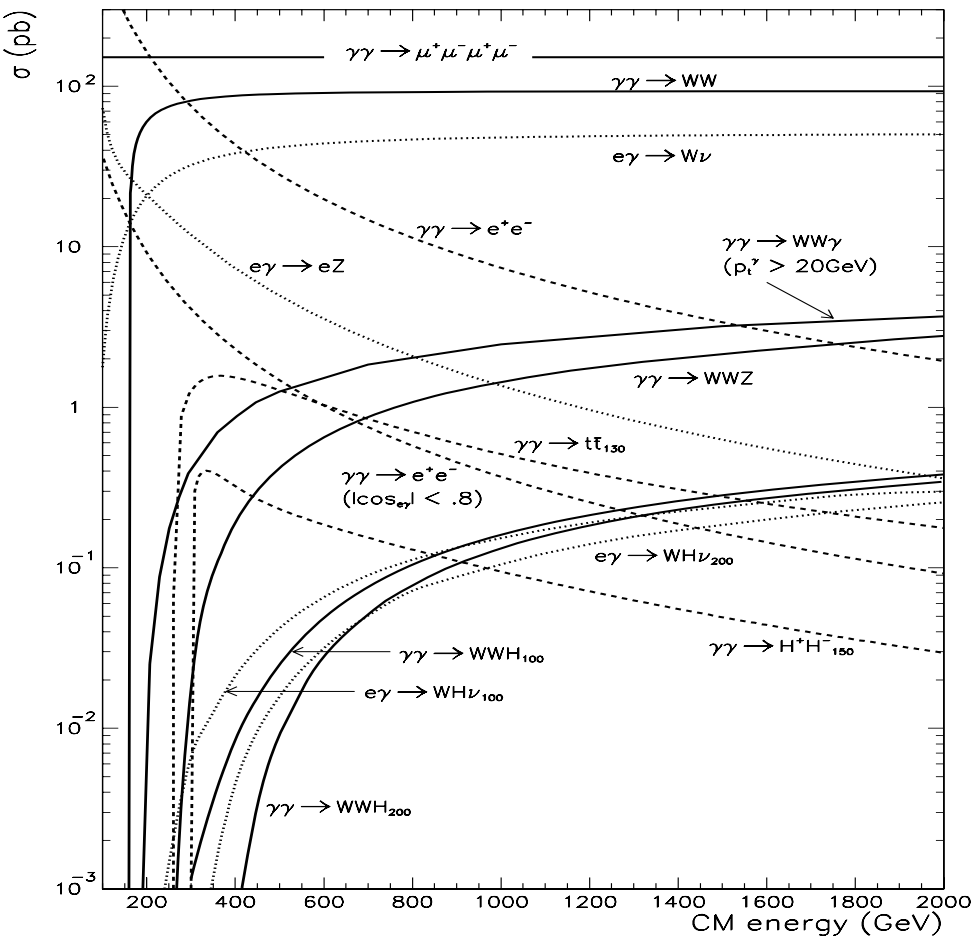

Figure A.2: *The cross sections of some processes in $\gamma\gamma$ and γe collisions.*

The PLC provides the best opportunity for study of t–quark properties themselves. Indeed, the cross section of $t\bar{t}$ production in the $\gamma\gamma$ collision is larger and it decreases more slowly with energy than that in e^+e^- collision (Fig. A.3). Therefore, relatively far from the threshold one can expect at PLC about 10^5 $t\bar{t}$ pairs per year, their decay products being overlapped weakly. Some rare t–decays could be studied here.

As mentioned in ref. [96], the PLC has a great advantage over e^+e^- collider for the study of heavy scalar superpartners such as the top squark, $\tilde{t}$. In e^+e^- collisions $\tilde{t}\bar{\tilde{t}}$ pairs would be produced in the kinematically suppressed p-wave and could not be effectively studied unless the available collider energy were much greater than the threshold production energy. In $\gamma\gamma$ collisions stop-antistop pairs are produced in the s-wave, which can be further enhanced by choosing photon beams of equal helicity.

A.2.5 The new physics

Two opportunities should be mentioned when we speak about effects of new physics — the discovery of new particles and new interactions of known particles. PLC provides

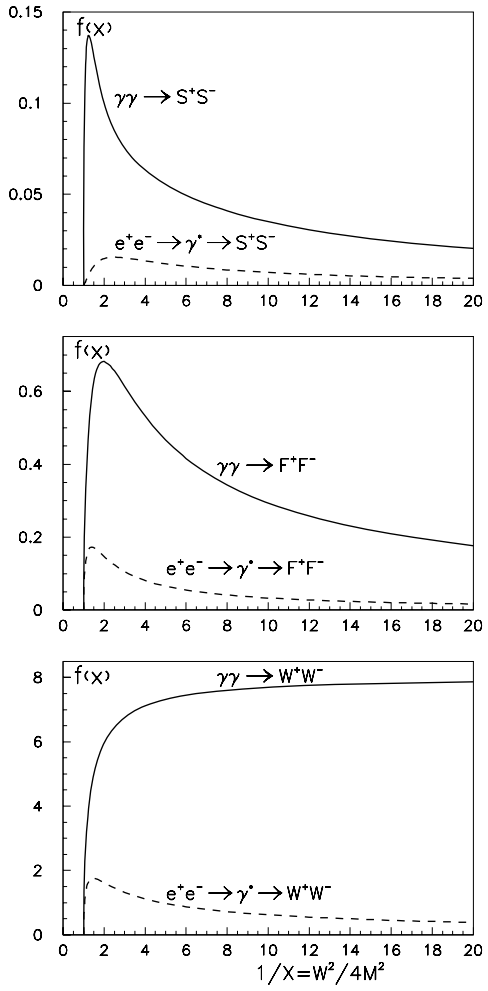

Figure A.3: *Comparison of cross sections for charged pair production in e^+e^- and $\gamma\gamma$ collisions. The cross section $\sigma = (\pi\alpha^2/M^2)f(x)$, P=S (scalars), F (fermions), W (W-bosons); M is particle mass, $x = W^2_{p\bar{p}}/4M^2$. The functions $f(x)$ are shown.*

the best place for discovering many new particles in comparison with other colliders of the same energy. It is connected with the following reasons:

(i) The signal to background (S/B) ratio at PLC is often much better than that at hadron colliders (for more details see ref. [97]).

(ii) In comparison with hadron colliders photons are "democratic" with respect to all charged particles.

(iii) The cross sections of charged particles production in $\gamma\gamma$ collisions are larger than those in e^+e^- collisions (see Fig. A.3). Even if PLC luminosity is 5 times less than that for basic e^+e^- linear collider, the number of pairs produced at e^+e^- collider is not greater than at $\gamma\gamma$ collider. Besides, these cross sections in $\gamma\gamma$ collision decrease

slower with growth of the energy. This provides an opportunity to study new particles relatively far from threshold with a substantial rate. In this region the decay products of these new particles are overlapped weakly. Therefore, their detailed study will be more feasible.

(iv) γe collisions offer additional opportunities, such as excited electron or neutrino production $\gamma e \to e^*$, $\gamma e \to \mathrm{W}\nu_e^*$, or single selectron production reaction $\gamma e \to \tilde{\gamma}\tilde{e}$.

The physics potential of PLC in discovering of new particles and interactions was considered in numerous papers (see also refs. [98], [39] –[46]). These include:

- SUSY particles [99]:
$$\gamma\mathrm{e} \to \tilde{\mathrm{W}}\tilde{\nu};\ \ \gamma\gamma \to \tilde{\mathrm{W}^+}\tilde{\mathrm{W}^-};\ \gamma\mathrm{e} \to \tilde{\mathrm{Z}}\tilde{e};\ \ \gamma\gamma \to \tilde{P}\tilde{P},\ (\tilde{P} \equiv \tilde{\ell},\ \tilde{H^{\pm}},\ \tilde{u},\ \tilde{d}).$$
- Excited leptons and quarks [100]:
$$\gamma e \to e^*; \qquad \gamma\gamma \to \ell^*\bar{\ell}; \qquad \gamma e \to \nu^*\mathrm{W}; \qquad \gamma\gamma \to q^*\bar{q}.$$
- Leptoquarks [101].
- Charged Higgses.
- Composite scalars and tensors.
- Dirac–Schwinger monopoles with mass $\lesssim 10E$ [102].
- Invisible axion (in the conversion region) [103, 104].
- Higgs nonstandard interactions [65, 66].
- The possibility to detect $\tilde{e}$ in the process $\gamma\mathrm{e} \to \tilde{\mathrm{Z}}\tilde{e}$ with a mass higher than in $\mathrm{e^+e^-}$ collisions (where $\tilde{e}^+\tilde{e}^-$ are produced in pairs), where $\tilde{\mathrm{Z}}$ is the lightest neutralino and $\tilde{e}$ decays into $\tilde{\mathrm{Z}}\tilde{e}$.

A.2.6 Hadron physics and QCD

Hadron physics and QCD are the traditional fields for the $\gamma\gamma$ collisions. The $\gamma\gamma$ experiments provide new type of collisions with the simplest quark structure of the pointlike initial state. The PLC will continue these studies to new regions. The results from PLC together with those from the Tevatron and HERA, will produce the entire set of data related to a factorized (in the old Regge sense) set of processes. In this respect, HERA gets a new importance of a bridge between PLC and Tevatron/LHC (see review [105] for some details).

The expected values of **the total cross section** $\sigma(\gamma\gamma \to hadrons)$ **and diffraction like processes in the soft region** are: $\sigma^{tot} \equiv \sigma_{\gamma\gamma\to hadrons} \sim 0.3\ \mu b$ in the SLC energy region, and $\sigma^{tot} \sim 0.5$–$1\ \mu b$ at $W_{\gamma\gamma} \sim 2$ TeV [106]. Besides, $\sigma(\gamma\gamma \to \rho^0\rho^0) \sim 0.1\sigma^{tot}$ (see [107]). The energy dependence of this cross section (together with the Q^2 dependence in γe collisions) in comparison to $\sigma_{pp}(\sigma_{p\bar{p}})$ and $\sigma_{\gamma p}$ will allow us to understand the nature of the growth of hadron cross sections with energy. The crucial problem is to test the possible factorization of these cross sections (this factorization is assumed in ref. [106]).

For semihard processes the nontrivial results in pQCD could be obtained almost without any model assumptions due to the simple pointlike nature of photons. The influence of hadronlike component of photon is expected to be relatively small at large

enough $p_\perp$ only. For example, for the diffraction like processes it is expected to be at $p_\perp > 7$ GeV [108].

The processes $\gamma\gamma \to \rho^0 X$, $\gamma\gamma \to \gamma X$, $\gamma\gamma \to \rho^0\phi$ with rapidity gap are described by pure Pomeron exchange. They present the best opportunity to study Pomeron. The processes $\gamma\gamma \to \pi^0 X$, $\gamma\gamma \to \pi^0 a_2$ with rapidity gap are described only by odderon exchange. They present a unique opportunity for odderon study. The cross sections of some processes, integrated over the range [3] of $p_\perp > 7$ GeV and with large enough rapidity gap, are estimated from below as [109, 110].:

$$\sigma_{\gamma\gamma\to\rho^0 X} \gtrsim 1\,\mathrm{pb}, \quad \sigma_{\gamma\gamma\to\gamma X} \gtrsim 0.2\,pb, \quad \sigma_{\gamma\gamma\to\pi^0 X} \gtrsim 0.4\,\mathrm{pb}\,.$$

The first two quantities should be multiplied by the growing BFKL factor (see [111, 112]).

Photon structure function is studied now at e^+e^- colliders. At PLC it will be studied in a new region and with high accuracy (see [113]).

A.3 Conversion region

A.3.1 Optimization of laser parameters, conversion efficiency

The generation of high energy γ-quanta by Compton scattering of the laser light on relativistic electrons is a well known method[114] and has been used in many laboratories. However, usually the conversion efficiency of electron to photons $k = N_\gamma/N_e$ is very small, only about 10^{-7}–10^{-5}. At linear colliders, due to small bunch sizes one can focus the laser more tightly to the electron beams and get $k \sim 1$ at rather moderate laser flash energy. The kinematics of Compton scattering for this case, cross sections, calculation of the conversion efficiency and consideration of various processes in the conversion region (pair creation, nonlinear effects) can be found in [2]-[5].

In the conversion region a laser photon with the energy ω_0 scatters at a small collision angle on a high energy electron with the energy E_0. The energy of the scattered photon ω depends on its angle ϑ relative to the motion of the incident electron as follows:

$$\omega = \frac{\omega_m}{1 + (\vartheta/\vartheta_0)^2}, \quad \omega_m = \frac{x}{x+1}E_0; \quad \vartheta_0 = \frac{mc^2}{E_0}\sqrt{x+1}; \tag{A.1}$$

where

$$x = \frac{4E\omega_0}{m^2c^4} \simeq 15.3\left[\frac{E_0}{\mathrm{TeV}}\right]\left[\frac{\omega_0}{eV}\right] = 19\left[\frac{E_0}{\mathrm{TeV}}\right]\left[\frac{\mu m}{\lambda}\right], \tag{A.2}$$

ω_m is the maximum energy of scattered photons (in the direction of the electron, Compton 'backscattering').

For example: E_0 =250 GeV, ω_0 = 1.17 eV (λ = 1.06 μm) (Nd:Glass laser) $\Rightarrow$ x=4.5 and $\omega/E_0 = 0.82$.

[3] It corresponds to the production angle above 70-100 mrad at PLC with $W_{\gamma\gamma}$ = 100–180 GeV.

The energy of the backscattered photons grows with increasing of x. However, at $x > 2(\sqrt{2}+1) \approx 4.8$ [2], high energy photons are lost due to e^+e^- creation in the collisions with laser photons. The maximum conversion coefficient (effective) at $x \sim 10$ is $k_{max} \sim 0.3$ [4], while at $x < 4.8$ it is about 0.65 (one conversion length). The luminosity in the latter case is increased by a factor 5. For $x = 20$ and $x = 4.8$ the difference is already of one order of magnitude. Further we will consider only the case $x \sim 4.8$, though higher x are also of interest for the experiments in which the ultimate monochromaticity of $\gamma\gamma$ collisions is required.

The wave length of the laser photons corresponding to $x = 4.8$ is

$$\lambda = 4.2 E_0[\mathrm{TeV}] \ \ \mu m. \tag{A.3}$$

For $2E_0 = 500$ GeV it is about 1 μm, that is exactly the region of the most powerful solid state lasers.

The energy spectrum of the scattered photons for $x = 4.8$ is shown in Fig. A.4 for various helicities of electron and laser beams (here λ_e is the mean electron helicity ($|\lambda_e| \leq 1/2$), P_c is the helicity of laser photons. We see that with the polarized beams at $2\lambda_e P_c = -1$ the number of high energy photons nearly doubles. This case we will use in further examples. The photon energy spectrum presented in Fig. A.4 corresponds to the case of small conversion coefficient. In the "thick" target each electron may undergo multiple Compton scatterings [5]. The secondary photons are softer in general and populate the low part of the spectrum.

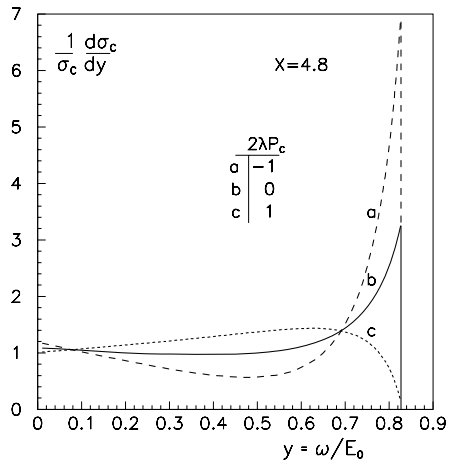

Figure A.4: *Spectrum of the Compton scattered photons for different polarizations of the laser and electron beams.*

The mean helicity of the scattered photons is shown in Fig. A.5 for various helicities of the electron and laser beams [5]. For $2P_c\lambda_e = -1$ (the case with good monochromaticity) all photons in the high energy peak have a high degree of like-sign

polarization. If the electron polarization is less than 100% and $|P_c| = 1$, nevertheless the helicity of the most high energy photon is still 100% , but the energy region with a high helicity becomes narrower. Low energy photons are also polarized, but due to contribution of multiple Compton scattering this region is not useful for the polarization experiments. The most valuable region for experiments is that near the maximum photon energy. Higher degree of longitudinal photon polarization is essential for suppression of the QED background in the search (and study) of the intermediate Higgs. Note that at 0.5 TeV ee collider the region of the intermediate Higgs can be studied with rather small x. In this case the helicity of scattered photons is almost independent on polarization of the electrons, and if $P_c = 1$ the high energy photons have very high circular polarization in wide range near the maximum energy even with $\lambda_e = 0$ [124].

The measurement of CP-parity of the Higgs boson in $\gamma\gamma$ collisions can be done using linearly polarized photons (sect.2). At $y = y_m$ the degree of linear polarization [3]

$$l_\gamma = \frac{2}{1 + x + (1+x)^{-1}}, \tag{A.4}$$

it is 33% at $x = 4.8$ and more than 80% at $x \leq 1$. Recently [47] it was suggested to transform circular polarization of high energy photons into linear without loss of intensity using an additional linearly polarized laser bunch. For this method additional studies are required.

For the calculation of the conversion efficiency it is useful to remember the correspondence between the parameters of the electron beam and laser beam: the emittance of the Gaussian laser bunch with diffraction divergence is $\epsilon_{x,y} = \lambda/4\pi$, the beta function at a laser focus $\beta \equiv Z_R$, where Z_R is known as the Rayleigh length in the optics literature. The r.m.s. spot size of a laser beam at the focus ($i = x, y$) [2]

$$\sigma_{L,i} = \sqrt{\frac{\lambda}{4\pi} Z_R}. \tag{A.5}$$

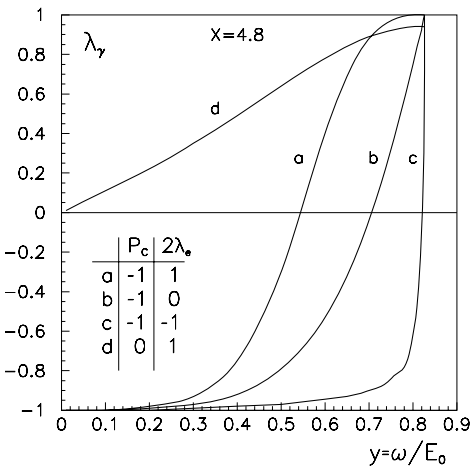

Figure A.5: *Mean helicity of the scattered photons.*

The r.m.s. transverse size of a laser near the conversion region depends on the distance z to the focus (along the beam) as $\sigma_{L,x}(z) = \sigma_{L,x}(0)\sqrt{1+z^2/Z_R^2}$. $2Z_R$ is then the effective length of the conversion region.

Neglecting multiple scattering, the dependence of the conversion coefficient on the laser flash energy A can be written as

$$k = N_\gamma/N_e \sim 1 - \exp(-A/A_0),$$

where A_0 is the laser flash energy for which the thickness of the laser target is equal to one Compton collision length. This corresponds to $n_\gamma \sigma_c l = 1$, where $n_\gamma \sim A_0/(\pi\omega_0 a_\gamma^2 l_\gamma)$, σ_c - is the Compton cross section ($\sigma_c = 1.8 \cdot 10^{-25}\ cm^2$ at $x = 4.8$), l is the length of the region with a high photon density, which is equal to $2Z_R$ at $Z_R \ll \sigma_{L,z} \sim \sigma_z$ (σ_z is the electron bunch length). This gives

$$A_0 = \frac{\pi\hbar c\sigma_z}{\sigma_c} = 5\sigma_z[\mathrm{mm}],\ J \quad \text{for} \quad x = 4.8. \tag{A.6}$$

Note that the required flash energy decreases with reducing the Rayleigh length up to σ_z, and it is hardly not changed with further decreasing of Z_R. This is because the density of photons grows but the length having a high density decreases and Compton scattering probability is almost constant. It is not helpful to make the radius of the laser beam at the focus smaller than $\sigma_{L,x} \sim \sqrt{\lambda\sigma_z/4\pi}$, which may be much larger than the transverse electron bunch size at the conversion region.

For a more precise optimization of laser parameters we have used the following formula for the conversion probability [31]

$$k = \frac{N_\gamma}{N_e} = 1 - \frac{1}{\sqrt{2\pi}\sigma_z}\int exp\ (-\frac{z^2}{2\sigma_z^2} - U(z))\ dz$$

$$\text{where}\ \ U(z) = \frac{2\sigma_c A}{\sqrt{2\pi}\pi c\hbar Z_R \sigma_{L,z}}\int \frac{exp\ (-\frac{2(s-z/2)^2}{\sigma_z^2})}{1+s^2/Z_R^2}\ \ ds \tag{A.7}$$

Here $\sigma_z, \sigma_{L,z}$ are the r.m.s. length of the electron and laser beams respectively, N_γ is the number of photons produced by the electrons in their first Compton scatterings (which can give photons with $\omega \sim \omega_{max}$).

For analyzing the conversion efficiency we have considered only the geometrical properties of the laser beam and the pure Compton effect. However, in the strong electromagnetic field at the laser focus, multiphoton effects (non-linear QED) are important. Nonlinear effects are described by the parameter [115, 104]

$$\xi = \frac{eF\hbar}{m\omega_0 c}, \tag{A.8}$$

where F is the r.m.s. strength of the electrical (magnetic) field in the laser wave. At $\xi^2 \ll 1$ an electron interacts with one photon (Compton scattering), while at $\xi^2 \gg 1$ an electron scatters on many laser photons simultaneously (synchrotron radiation in a wiggler).

The transverse motion of an electron in the electromagnetic wave leads to an effective increase of the electron mass: $m^2 \to m^2(1+\xi^2)$, and the maximum energy of the scattered photons decreases: $\omega_m = x/(1+x+\xi^2)$. At $x = 4.8$ the value of ω_m/E_0 decreases by 5% at $\xi^2 = 0.3$ [5]. This value of ξ^2 we take as the limit. In the conversion region at $z = 0$

$$\xi^2 = \frac{4r_e\lambda A}{(2\pi)^{3/2}\sigma_{L,z}mc^2 Z_R} \tag{A.9}$$

The results of the calculation of N_γ/N_e for various values of the flash energy and beam parameters are presented in Fig. A.6. The points on the curves correspond to $\xi^2 = 0.3$ (at $\lambda = 1$ μm, optimum for $2E_0 = 500$ GeV). These points limit the minimum values of Z_R. Fig. A.6 may be used for other beam energies. According to eq.(6), A_0 depends only on the electron bunch length and Compton cross section (which is constant, if x is kept constant). The value of $Z_{R,min} \propto \lambda$ (see eq.(9))

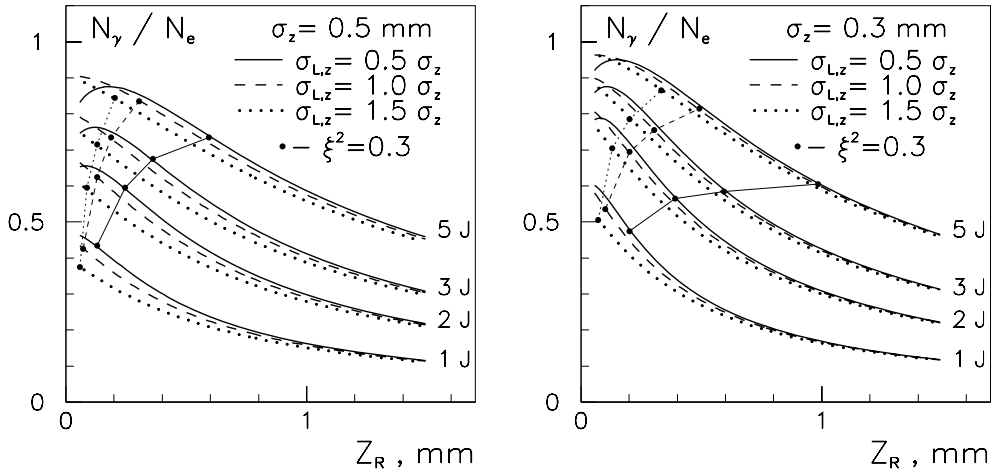

Figure A.6: *Conversion efficiency vs Z_R for various values of the flash energy and photon bunch length. Left figure for electron bunch length $\sigma_z = 0.5$ mm (TESLA), right for $\sigma_z = 0.3$ mm (SBLC).*

The requirements for the laser parameters for $N_\gamma/N_e = 1 - e^{-1} = 0.632$ (one collision length) are summarized in Table A.1. The second values of Z_R correspond approximately to a 10% drop in conversion efficiency.

For the removal of disrupted beams at photon colliders it is necessary to use a crab crossing beam collision scheme (see Fig. A.9 in the next section). In this scheme the electron beam is tilted relative to its direction of motion by an angle $\alpha = \alpha_c/2 \sim$ 15 mrad. This means that in the laser focus region the electron beam has an effective size $\sigma_x = \sigma_z\alpha_c/2$, that is 7.5 and 4.5 μm for TESLA and SBLC respectively. These sizes are comparable to, and for TESLA even larger than the laser spot size (see Table 1). Therefore, for the equal conversion efficiency one has to increase the laser flash energy

by a factor of 1.9–1.5 respectively. The other possible solution is the crab crossing collisions of the electrons and laser bunches [116]. The tilt of the laser bunch can be obtained using "chirped" laser pulses and grating as discussed in sect.7.1. This solution is straightforward for solid state lasers, which in any case use chirped pulses. For some schemes of free electron laser this also can be done easily. For for simplicity we will take conservative values of the required flash energies: SBLC - 2 J, TESLA - 4 J.

Table A.1: *Required energy (A_0) and duration of laser flash ($\sigma_{L,z}$ for various length of the electron bunch (σ_z,) at $\lambda = 1$ μm, $x = 4.8$. Z_R and $\sigma_{L,x}$ are optimum Rayleigh length and r.m.s. size of the focal region.*

σ_z, mm	A_0, J	$\sigma_{L,z}$, mm	Z_R, mm	$\sigma_{L,x}$, μm
0.3	1.5	0.3	0.15–0.2	3.5–4
0.5	2.1	0.5	0.15–0.25	3.5–4.5
0.7	2.8	0.7	0.15–0.3	3.5–5

As follows from Fig. A.6 the nonlinear effects at $2E = 500$ GeV ($\lambda_{opt} = 1$ μm) and σ_z =0.3–0.7 mm have a small influence to the required laser flash energy. For shorter electron bunches and larger λ the required flash energy due to nonlinear effects may be much larger than deduced from the diffraction consideration only [5]. Recently [29] it was shown how the problem of nonlinear effects at the conversion region can be avoided. Owing to non-monochromaticity of a laser light it is possible to 'stretch' the depth of a laser focus keeping the radius of the focal spot size constant. In this scheme the required flash energy is determined only by the diffraction and is given approximately by eq.(6).

A.3.2 Low energy electrons after conversion.

For the removal of the spent electrons it is important to know the values of the maximum disruption angle and minimum energy of the spent electrons. The disruption angles are created during beam collisions at the IP. The electrons with the lower energies have larger disruption angles. The simulation code (to be described in the next section) deals with about 5000 (initial) macroparticles and can not describe the distribution tails. But providing the minimum energy and energy dependence of the disruption angle are known, we can correct the value of maximum disruption angle obtained by the simulation.

Low energy electrons are produced at the conversion region due to multiple Compton scatterings[4]. Fig. A.7 shows the probability that an electron which has passed the conversion region has the energy below E/E_0. Two curves were obtained by simulation of 10^5 electrons passing the conversion region with the thickness 1 and 1.5 of the Compton collision length (at $x = 4.8$). Extrapolating these curves (by tangent line)

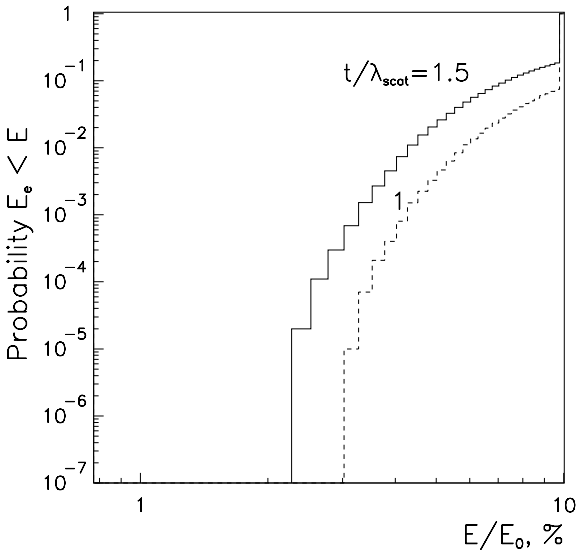

Figure A.7: *Probability for an electron after the conversion region to have an energy below* E/E_0.

to the probability 10^{-7} we can obtain the minimum electron energy corresponding to this probability: 2.5% and 1.7% of E_0 for $t/\lambda_{scat} = 1$ and 1.5 respectively. The ratio of the total energy of all these electrons to the beam energy is about $2 \cdot 10^{-9}$. This is a sufficiently low fraction comparable with other backgrounds (see sec.5). So, we can conclude that the minimum energy of electrons after the conversion region is about 2% of initial energy, in agreement with the analytical estimation [4].

A.4 Interaction region

A.4.1 Collision schemes

We will consider two basic collision schemes (Fig. A.8):

Scheme A ("without deflection"). There is no magnetic deflection of spent electrons and all particles after conversion region travel to the IP [12, 19]. The conversion point may be situated very close to the IP at the distance $b \sim 5\sigma_z$.

Scheme B ("with deflection"). After conversion region particles pass through a region with a transverse magnetic field where electrons are swept aside [2, 4, 5]. Thereby one can achieve a more or less pure $\gamma\gamma$ or γe collisions.

The scheme A is simpler but background conditions are much worse and disruption angles are larger. Additional background is connected not only due to mixture of different types of collisions but also due to emission of a huge number of beamstrahlung photons during beam collision. This leads to "background" $\gamma\gamma$ and γe luminosities at small invariant masses exceeding the "useful" luminosity in the high energy peak by

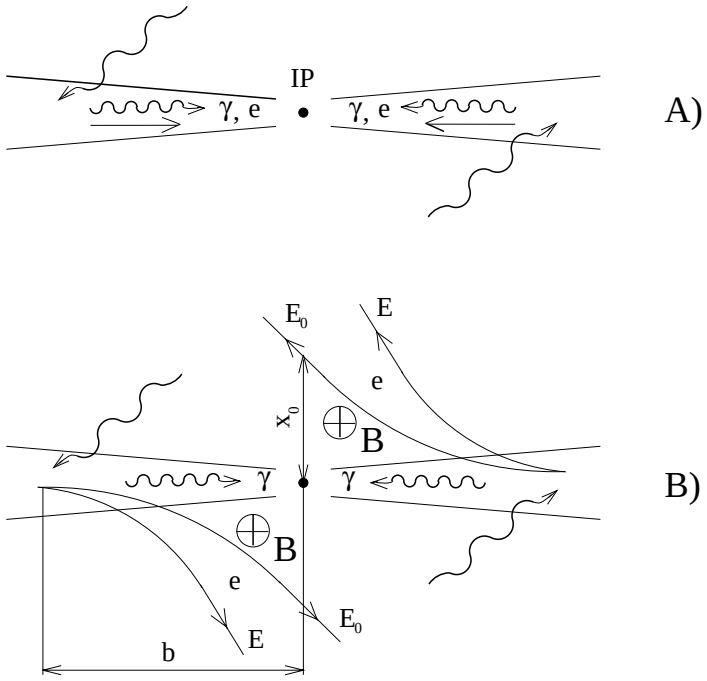

Figure A.8: *Two basic collision schemes: a) "without deflection", b) "with deflection" using the sweeping magnet.*

one order. This causes an additional backgrounds to the detector (see sect.5).

In both schemes the removal of the disrupted spent beams can best be done using the crab-crossing scheme[117] (Fig. A.9), which is proposed in the NLC and JLC projects for e^+e^- collisions. In this scheme the electron bunches are tilted (using RF cavity) with respect to the direction of the beam motion, and the luminosity is then the same as for head-on collisions. Due to the collision angle the outgoing disrupted beams travel outside the final quads. In the next sections both schemes will be considered in detail.

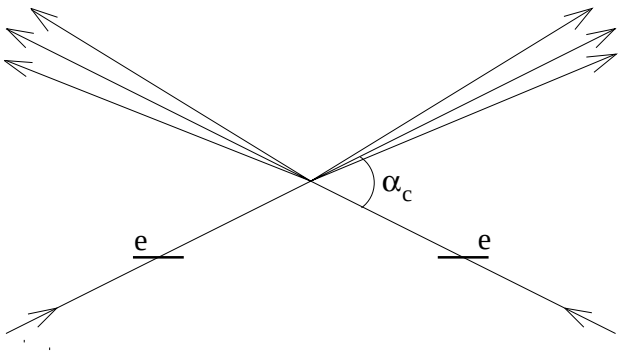

Figure A.9: *Crab-crossing scheme.*

A.4.2 Collision effects in $\gamma\gamma$ and γe collisions

.

Luminosity in $\gamma\gamma$,γe collisions is restricted by many factors:

- collision effects (coherent pair creation, beamstrahlung, beam displacement);
- beam collision induced backgrounds (large disruption angles of soft particles);
- luminosity induced backgrounds (hadron production, e^+e^- pair production);
- problem of obtaining electron beams with small emittances.

For optimization of the photon collider it is useful to know qualitatively the main dependences. In this section we will consider collision effects which restrict the luminosity [4, 5].

It seems, at first sight, that there are no collision effects in $\gamma\gamma$ and γe collisions because at least one of the beams is neutral. This is not completely correct because during beam collisions electrons and photons are influenced by the field of the oppositely moving electron beam. In $\gamma\gamma$ collisions it is spent beams, in γe collisions the field is created also by the "main" electron beam used for γe collisions.

A strong field leads to the following effects.
In $\gamma\gamma$ collisions: conversion of photons into e^+e^- pairs (coherent pair creation[11]).
In γe collisions: a) coherent pair creation; b) beamstrahlung; c) beam displacement.

$\gamma\gamma$ collisions.
Coherent pair creation is exponentially suppressed for $\Upsilon = \gamma B/B_0 \leq 1$ ($B_0 = m^2c^3/e\hbar = 4.4 \cdot 10^{13}$ Gauss). But, if $\Upsilon > 1$, most of high energy photons can be converted to e^+e^- pairs during the beam collision [4]. There are two ways to avoid this effect (i.e. to keep $\Upsilon \leq 1$):
1) to use flat beams;
2) to deflect the electron beam after conversion at a sufficiently large distance (x_0 for $E = E_0$) from the IP.

The condition $\Upsilon < 1$ corresponds approximately to the condition [5]

$$x_0 \text{ or } \sigma_{x,min} \geq 1.5\frac{Nr_e^2\gamma}{\alpha\sigma_z} \sim 30\left(\frac{N}{10^{10}}\right)\frac{E_0[TeV]}{\sigma_z[mm]}, \text{ nm} \qquad \text{(A.10)}$$

For TESLA and SBLC $x_0, \sigma_{x,min} \geq 217(110)E_0[TeV]$ nm respectively.

In the scheme with flat beams, the minimum vertical beam size is $\sigma_{\gamma,y} \sim b/\gamma$, where $b \geq 5\sigma_z$ (not 1-2σ_z because the field in the conversion region should be small). But, if σ_y of the electron beam is larger than this value, then it is reasonable to choose $b/\gamma \sim \sigma_y$. This case is relevant for TESLA and SBLC. The maximum luminosity in this case is

$$L_{\gamma\gamma} \sim \frac{k^2N^2f}{4\pi\sigma_{x,min}\sigma_{\gamma,y}} = \frac{k^2N\alpha\sigma_z f}{6\pi r_e^2\sigma_{\gamma,y}\gamma}, \qquad \text{(A.11)}$$

where $\sigma_{\gamma,y} = max(\sigma_y, 5\sigma_z/\gamma)$.

If the available σ_x is much smaller than $\sigma_{x,min}$ given by eq.(10), then it is reasonable to keep σ_x as small and to provide $\Upsilon < 1$ by deflecting beam on the distance x_0 given by eq.(10). The minimum photon spot size in this case is

$$\sigma_{\gamma,min} \sim b/\gamma \sim \sqrt{\frac{2E_0x_0}{eB_e}}\frac{1}{\gamma} \sim \sqrt{\frac{3Ner_e}{\alpha\sigma_z B_e}} \sim 7.5\left(\left[\frac{N}{10^{10}}\right]\left[\frac{mm}{\sigma_z}\right]\left[\frac{T}{B_e}\right]\right)^{1/2}, \quad \text{nm} \tag{A.12}$$

where B_e is the transverse magnetic field in the region between the CP and IP. For "nominal" TESLA(SBLC) parameters (see sect 4.4) $\sigma_{\gamma,min} \sim 20(14)$ nm at $B = 1$ T. Such photon spot can be obtained only when electron bunch sizes are smaller than these values. The maximum luminosity in this case is

$$L_{\gamma\gamma} \sim \frac{k^2N^2f}{4\pi\sigma^2_{\gamma,min}} = \frac{k^2N\alpha\sigma_z f B_e}{12\pi e r_e} \tag{A.13}$$

However, with the horizontal emittances considered currently in the TESLA and SBLC projects the level $\sigma_x \sim 15$ nm is unreachable. In the case $\sigma_x > \sigma_{\gamma,min}$

$$L_{\gamma\gamma} \sim \frac{k^2N^2f}{4\pi\sigma_{\gamma,min}\sigma_x} = \frac{k^2N^2f}{4\pi\sigma_x}\sqrt{\frac{\alpha\sigma_z B_e}{3Ner_e}} \tag{A.14}$$

We have considered all cases important for optimization of $\gamma\gamma$ collisions. Fo given attainable σ_x and σ_y one can check which scheme gives larger liminosity. Final optimization should be done by simulation. Note that in all cases, even for $\sigma_x > \sigma_{x,min}$, some magnetic deflection is useful for reduction of backgrounds.

All described above is valid for any collider parameters. But there is one nice surprise: at $2E_0 = 500$ GeV and with the TESLA–SBLC parameters there exists no coherent pair creation (due to beam repulsion), and one can then obtain very high $\gamma\gamma$ luminosity which is only determined by the attainable emittances of electron beam [24] (for more detail see sect.4.5.3 "Ultimate luminosity").

γe collisions

In γe collisions there are more collision effects (coherent pair creation, beamstrahlung and beam displacement), the detail consideration of these effects and calculation of the γe luminosity can be found elsewhere[5]. Briefly, the picture is the following.

1) To avoid coherent pair creation the electron beams should be flat, with σ_x larger than it is given by eq.(10).

2) By choosing the distance $b > \gamma\sigma_y$ we can obtain very monochromatic γe collisions.

3) To maintain good monochromaticity, the beamstrahlung losses of the "main" electron beam in the field of the spent beam should be small. This can be provided by magnetic deflection of the spent beam.

4) At low beam energies it can happen that due to repulsion the "main" electron beam is shifted and does not collide with the high energy photons. Therefore, the magnetic deflection of the spent electron beam should be kept large enough.

To meet all the above enumerated requirements the distance between the CP and IP in γe collisions must usually be larger than in $\gamma\gamma$ collisions, therefore the maximum attainable γe luminosity is somewhat smaller. In the scheme without magnetic

deflection one can also obtain a sufficiently large γe luminosity, but with much worse quality of collisions. The corresponding luminosity spectra are obtained by simulation in sect.4.5.

Disruption angles

The maximum disruption angle is an important issue for photon colliders determining the value of the crab crossing angle.

One source of large angle particles is low energy electrons from the conversion region and the minimum energy of these electrons is about $0.02E_0$ (sect.3.2). In the scheme without magnetic deflection the soft electrons are deflecting by the opposing beam by an angle [4]

$$\vartheta_d \sim 0.7\left(\frac{4\pi r_e N}{\sigma_z \gamma_{min}}\right)^{1/2} \sim 2\left(\frac{N/10^{10}}{\sigma_z[\text{mm}]E_0[\text{TeV}]}\right)^{1/2} \text{ mrad} \quad \text{for } E_{min} = 0.02E_0. \quad \text{(A.15)}$$

The coefficient 0.7 here was found by tracking particles in the field of the beam with a Gaussian longitudinal distribution for the TESLA–SBLC range of parameters. For $2E_0 = 500$ GeV for TESLA (SBLC) $\vartheta_d = 9(8)$ mrad .

One can decrease ϑ_d by predeflecting the spent electron beam by the external magnetic field. Unfortunately the kick angle (on the opposing beam) changes very slowly up to the displacement at IP $\Delta y \sim \sqrt{r_e N \sigma_z/\gamma_{min}}$. It is about 2.5 μm for the TESLA and 1 μm for SBLC for $E_{min} = 0.02E_0$. For this impact distance the kick angle decreases by a factor 1.7 only. At $b = 1.5$ cm the required B_e is 3.7(1.5) kGs for TESLA(SBLC). For larger fields the disruption angle decreases as $1/B_e$.

The second source of soft particles is hard beamstrahlung. The deflection angle is described by the same eq.(15), but with coefficient 1.2 instead of 0.7, which corresponds to the case when hard photon is emitted near the center of opposing beam. What is the minimum energy of electrons after beamstrahlung? According to Sokolov-Ternov formula the high energy tail is expressed as $exp(-\xi_S)$, where $\xi_S = 2y/(3\Upsilon(1-y))$ and $y = \omega/E$. As soon as the total number of radiated photons is of the order of one, this expression gives approximately the relative number of electrons with the energy loss above y. The probability 10^{-7} corresponds to $\xi_S = 16$. For $\Upsilon = 1$, which is maximum for photon colliders, we find $1 - y_{max} = 0.04$. In other words the lowest energy of electrons after beamstrahlung is about 4% of E_0 (for Υ =1).

According to eq.(15) with the coefficient 1.2 the deflection angle of such electrons (for $\Upsilon = 1$) will be larger by 20% than that for low energy electrons arising at the conversion region and $\vartheta_d \propto \sqrt{\Upsilon}$. The magnetic deflection decreases the disruption angles of the low energy electrons coming from the conversion region, however it does hardly changes almost the disruption angles of soft "beamstrahlung" electrons created by high energy electrons which have small magnetic deflection and pass the IP close to the opposing beam. The presented picture of collision effects helps to understand numerical results of the simulation.

A.4.3 Simulation code.

As we have seen, the picture of beam collisions in photon colliders is so complicated that the best way to see a final result is a simulation. In the present study we used the code written by V.Telnov[5, 118].

It is written for the simulation of e^+e^-, ee, γe, $\gamma\gamma$ beam collisions at linear colliders and takes into account the following processes:

1. *Multiple Compton scattering in the conversion region.* In the present simulation "good" case of polarization ($2P_c\lambda_e = -1$) was assumed and the thickness of the photon target was put equal to one conversion length.

2. *Deflection by the external magnetic field and synchrotron radiation* in the region between the CP and IP.

3. *Electromagnetic forces, coherent pair creation and beamstrahlung* during beam collisions at the IP.

4. *Incoherent e^+e^- creation in $\gamma\gamma$, γe, ee collisions.*

Initial electron beams are described by about 3000 macroparticles (m.p.) which have a shape of flat rectangular bars with sizes (x·y) equal to $0.4\sigma_x \cdot 0$. In the longitudinal direction the electron bunch has a Gaussian shape ($\pm 3\sigma$) and is cut on 150 slices. The macroparticles have only the transverse field and influence on macroparticles of the opposite bunch which have the same z-coordinate (this coordinate changes by steps). At initial positions macroparticles are directed to the collision region in the way corresponding to beam emittances and beta functions. During the simulation new macroparticles (photons, electrons and positrons) are produced which are considered further in the same way as the initial macroparticles.

At the output the code gives all parameters of colliding pairs (macroparticle "collides" when the distance between their centers is less then $0.15\sigma_x$ on x and less then $0.15\sigma_y$ on y–directions) and all parameters of the final particles. Incoherent e^+e^- pairs are simulated separately after beam collisions.

The code was used for simulation of the NLC based photon collider[31] and the results are in agreement [119] with the code GAIN[120] written later for the same purposes.

A.4.4 Parameters of electron beams

The parameters of electron beams considered for $\gamma\gamma$,γe collisions are presented in Table A.2.

Some comments:
TESLA(1) — is the basic variant considered for e^+e^- collisions at the TESLA.
TESLA(2) — is the second basic TESLA set of parameters for e^+e^- collisions with reduced vertical emittance.
TESLA(3) — as TESLA(1), but the horizontal emittance is reduced by a factor of 3.5;

Table A.2: *Parameters of electron beams.*

	TESLA(1)	TESLA(2)	TESLA(3)	TESLA(4)	SBLC(1)	SBLC(2)
$N/10^{10}$	3.63	1.82	3.63	3.63	1.1	1.1
σ_z, mm	0.5	0.5	0.5	0.5	0.3	0.3
f_{rep}, Hz	5	4	5	5	50	50
n_b	1130	2260	1130	1130	333	333
Δt_b, ns	708	354	708	708	6	6
$\gamma\epsilon_{x,y}/10^{-6}$, m·rad	14., 0.25	12., 0.03	4., 0.25	1., 1.	5., 0.25	0.5, 0.5
$\beta_{x,y}$, mm at IP	3.2, 0.5	3.2, 0.5	2.0, 0.5	1.1, 0.5	2.5, 0.4	0.77, 0.3
$\sigma_{x,y}$, nm	303, 16	280, 5.5	128, 16	47, 32	160, 14	28, 17.5
$L(geom), 10^{33}$	12.2	15.4	30.0	39	7.1	32.6

that may be achieved with optimized damping rings.
TESLA(4) — the variant with a low emittance polarized RF-gun (without damping rings). The emittances used here are by a factor of 5 lower than presently achieved for this number of particles [121]. However, it seems possible to join (using some difference in energies) many (5-10) low current beams with low emittances to one beam with the number of particles as in TESLA (1,3) variants.
SBLC(1) — is the basic variant considered for e^+e^- collisions at the SBLC.
SBLC(2) — the variant with a low emittance polarized RF-guns (see comment for TESLA(4))

For demonstration of ultimate parameters of the photon collider based on the TESLA we will consider also the "super" variant TESLA(4), where in comparison with TESLA(4) the emittances are further reduced by a factor 5. Such emittance of electron beams can be achieved using the method of laser cooling proposed recently[29]. This method requires lasers with the flash energy about 10 J (by a factor 3-4 larger than for $e\rightarrow\gamma$ conversion) which seems possible in the scheme having a laser photon recirculation. In this proposal we do not consider this option in the "main list".

As was noted before the electron beams in $\gamma\gamma$ collisions can have smaller horizontal beam sizes than in e^+e^- collisions. Beta functions presented in Table 2 are minimum for given beam parameters. In some case they are larger than σ_z due to Oide effect (chromatic aberrations due to synchrotron radiation in the final quads). We assumed that the final focusing system has the same structure as for e^+e^- collisions and the distance between IP and the nearest quad is 2 m.

Due to beam collisions at large collision angle the final quads should have a special design with a "hole" for disrupted beams. Moreover, the magnetic field in this region should be kept small enough (< 0.05 T), so that particles with the lowest energy (about 5 GeV) get a small deflection and follow essentially in the direction of the beam dump.

One possible solutions is to use a superconducting ironless quadrupole with concentric current of opposite polarities proposed for NLC[31]. The outer radius of the coils in this design is 3 cm. So, the minimum crossing angle is about 4/200 rad + disruption angle ($\sim$ 10 mrad), that is about 30 mrad. This is the value of crab crossing angle we

will use in our considerations. Others quad designs with iron poles are also possible. Low field region in this case can be arranged inside the quad using magnetic screens.

A.4.5 Simulation results

A.4.5.1 Scheme without deflecting magnets

In the scheme without sweeping magnets there is only one free parameter: the distance between the CP and IP. It is reasonable to take $b = 1.5\gamma\sigma_y$. For such b the spectral luminosity for hard photons is almost the same as for $b = 0$, but the low energy part of $\gamma\gamma$ luminosity is suppressed (because the spot size for low energy photons at the IP is larger than that for high energy photons). With this choice the value of b varies between 0.4–2.4 cm for the considered beam parameters. It was assumed that the thickness of laser target is equal to one collision length (for electrons with the initial energy) that corresponds to $k = 0.63$.

The results of simulation for $\gamma\gamma$, γe and ee luminosities are presented in Fig. A.10 and Table A.3 (second lane). All luminosity distributions are normalized to the geometrical luminosity $L_{geom} = N^2 f/(4\pi\sigma_x\sigma_y)$. Looking to these data one can see:

a) $L_{\gamma e}$(total) $\sim L_{\gamma\gamma}$(total) and $L_{\gamma e}(z > 0.65) \sim$ (1–2)$L_{\gamma\gamma}(z > 0.65)$; so $\gamma\gamma$, γe collisions can be studied simultaneously;

b) $L_{\gamma\gamma}$(total) $\sim 10 L_{\gamma\gamma}(z > 0.65)$; low energy $\gamma\gamma$ luminosity will give additional backgrounds;

c) $L_{ee} < 0.1\ L_{\gamma\gamma}$; (due to beam repulsion);

d) $L_{\gamma\gamma}(z > 0.65) =$ (1.2–3.3)10^{33} cm^{-2}s^{-1};

e) $N(\gamma\gamma \to$ hadrons$)$/collision $\sim$0.1–2 with $\overline{W_{\gamma\gamma}} \sim 0.15 \cdot 2E_0$.

f) maximum disruption angles $\vartheta_x, \vartheta_y < 10$ mrad.

We see that in the scheme without magnetic deflection there is mixture of $\gamma\gamma$, γe, ee collisions and most of collisions have small invariant masses. This low energy luminosity is produced by the soft photons after multiple Compton scattering and beamstrahlung photons created during beam collision.

A.4.5.2 Scheme with magnetic deflection

$\gamma\gamma$ collisions

Magnetic deflection allows having pure $\gamma\gamma$ collisions and suppress γe, ee backgrounds. It is important to note also that deflection of spent electrons can significantly suppress low energy $\gamma\gamma$ luminosity. The swept electron beam radiates many beamstrahlung photons in the field of the opposing spent electron beam but now these photons are not collided with particles from the opposing beam.

The optimization in this case consists of selection of CP–IP distance b and a value of the magnetic field B_e. This choice was done using the following requirements and arguments:

a) as soon as $\sigma_y < \sigma_x$ it is easier to deflect beams in the vertical direction;

b) $b > 1.5\gamma\sigma_y$ (to suppress low energy luminosity);

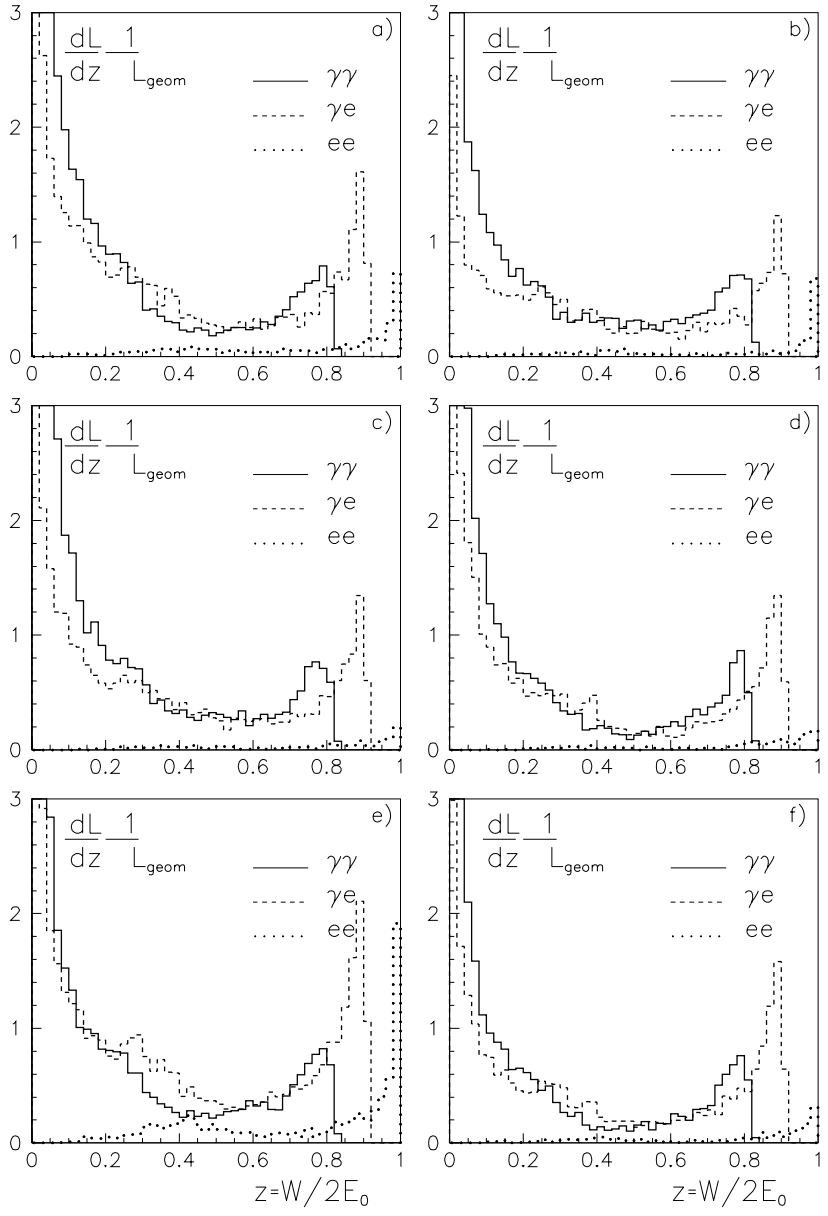

Figure A.10: *Luminosity spectra for the scheme without deflection for the $\gamma\gamma$ collider parameters presented in Tables A.2, A.3 (Figs. A.10a), b)... correspond to TESLA(1), TESLA(2)...). Luminosity distributions are normalized to the geometrical luminosity. For additional comments see the text.*

c) the deflection at the IP $\Delta_y > 4\sigma_y$ (to avoid collision with beamstrahlung photons);

d) the electromagnetic field at the IP should be below the threshold of the coherent e^+e^- creation ($\Upsilon < 1$).

e) b>1.5 cm (because the minimum distance of any material to the IP should be larger than 1 cm, that is determined by synchrotron radiation from the final quads (r<6 mm) and by low energy positrons which get kick in the field of opposing beam and spiraling in the vacuum chamber (see sect.5 for details).

It turns out that it is possible to meet all these requirements using $B_e \sim 0.5$ T. Such field can be produced by thin pulse magnet surrounding the IP (see sect.4.8). The results on $\gamma\gamma$ collisions in the scheme with deflection are shown in Fig. A.11 and summarized in Table A.3 (lane 3). One can see the following:

a) at high invariant masses $L_{\gamma\gamma}$(defl.)$\sim L_{\gamma\gamma}$(no defl.); but the total $L_{\gamma\gamma}$(defl.)$\sim$ 0.2–0.3 $L_{\gamma\gamma}$(no defl.) and one can expect smaller hadronic backgrounds (see sect.5);

b) $L_{\gamma e}(z > 0.65) \ll L_{\gamma\gamma}(z > 0.65)$;

c) L_{ee} is negligibly small;

d) the disruption angles are less than about 5 mrad (10 mrad without deflection).

γe collisions

We have seen that in the scheme without magnetic deflection, γe collisions with a large luminosity can be obtained simultaneously with $\gamma\gamma$ collisions. For some experiments it may be desirable to have pure γe collisions (at least in the region of the high energy peak). This can be done using sweeping magnets.

For optimization of γe collisions with sweeping magnets we use the following criteria:

a) the spent electrons should be deflected in a horizontal direction (larger beam size) because the "main" electron beam is shifted during the collision with the opposing spent electron beam and this shift should be smaller than the corresponding beam size. To avoid direct collision of beams we have to provide larger magnetic deflection than in the case of $\gamma\gamma$ collision that needs larger distance between CP and IP;

b) it should be checked that the process of coherent pair creation is below threshold ($\Upsilon < 1$) and broadening of the luminosity spectrum due to beamstrahlung is rather small;

c) as before we assumed B=0.5 T (at larger fields (and smaller b) the $L_{\gamma e}$ is somewhat larger, by 20-50%). The distance b between CP and IP was chosen as some compromise between the point with highest $L_{\gamma e}$ in the high energy peak and the point where background is small enough.

The results on γe luminosity (and $\gamma\gamma$, γe backgrounds) with the horizontal deflection are presented in Fig. A.12. and in Table A.3 (lane 4). Looking to these date one can make the following observations.

- γe luminosity spectrum is very monochromatic, the full width at the half of the maximum is about 5%.
- $L_{\gamma e}(z > 0.65) \sim$ (1.3–5.2)10^{33} cm^{-2}s^{-1}, approximately the same as without deflection, but now it is more monochromatic and almost without backgrounds.

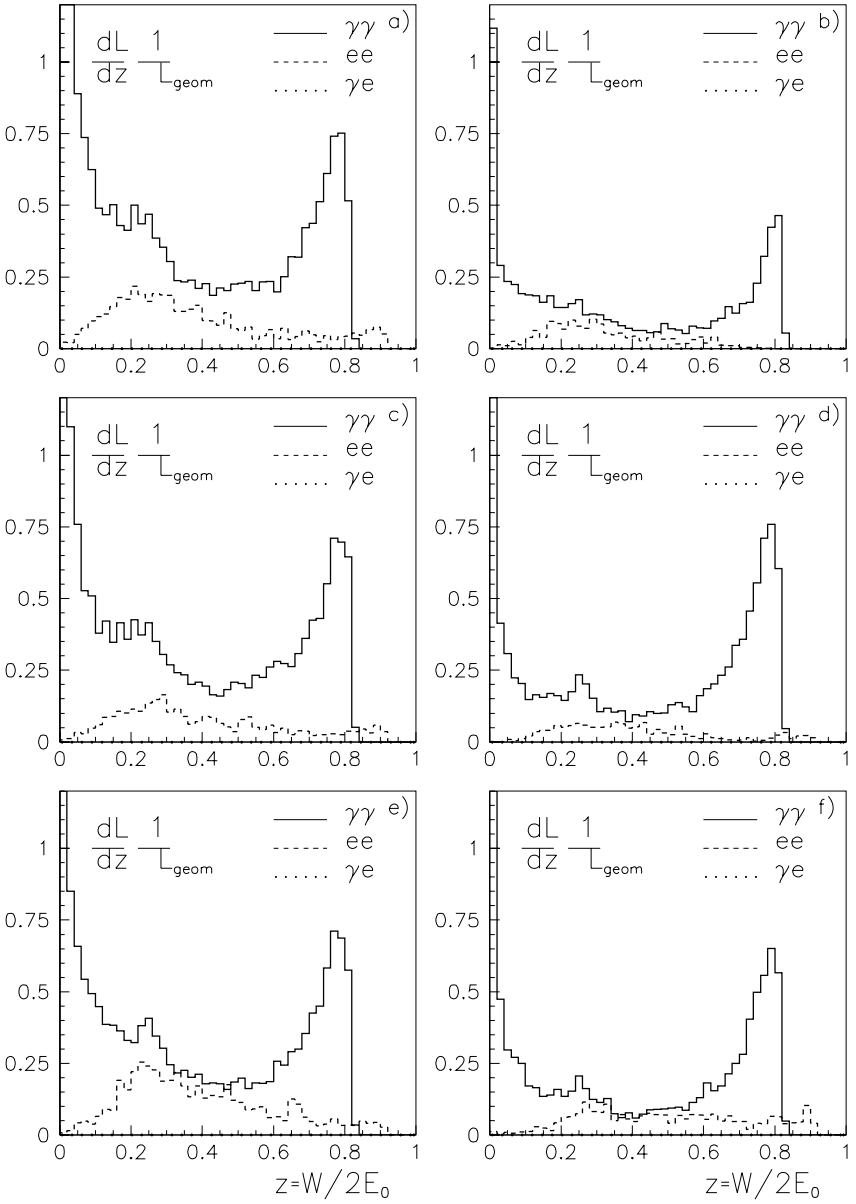

Figure A.11: *Spectral $\gamma\gamma$ luminosity in the scheme with the vertical deflection for the beam parameters presented in Tables A.2, A.3 (Figs. A.11a), b)... correspond to TESLA(1), TESLA(2)...). For additional comments see the text.*

- In all cases there is unremovable low energy $\gamma\gamma$ luminosity. It is due to collisions of the beamstrahlung photons (emitted by the "main" electron beam) with opposing high energy Compton photons. One should also add collisions of virtual (equivalent) photons with Compton photons which are not shown in our figures.

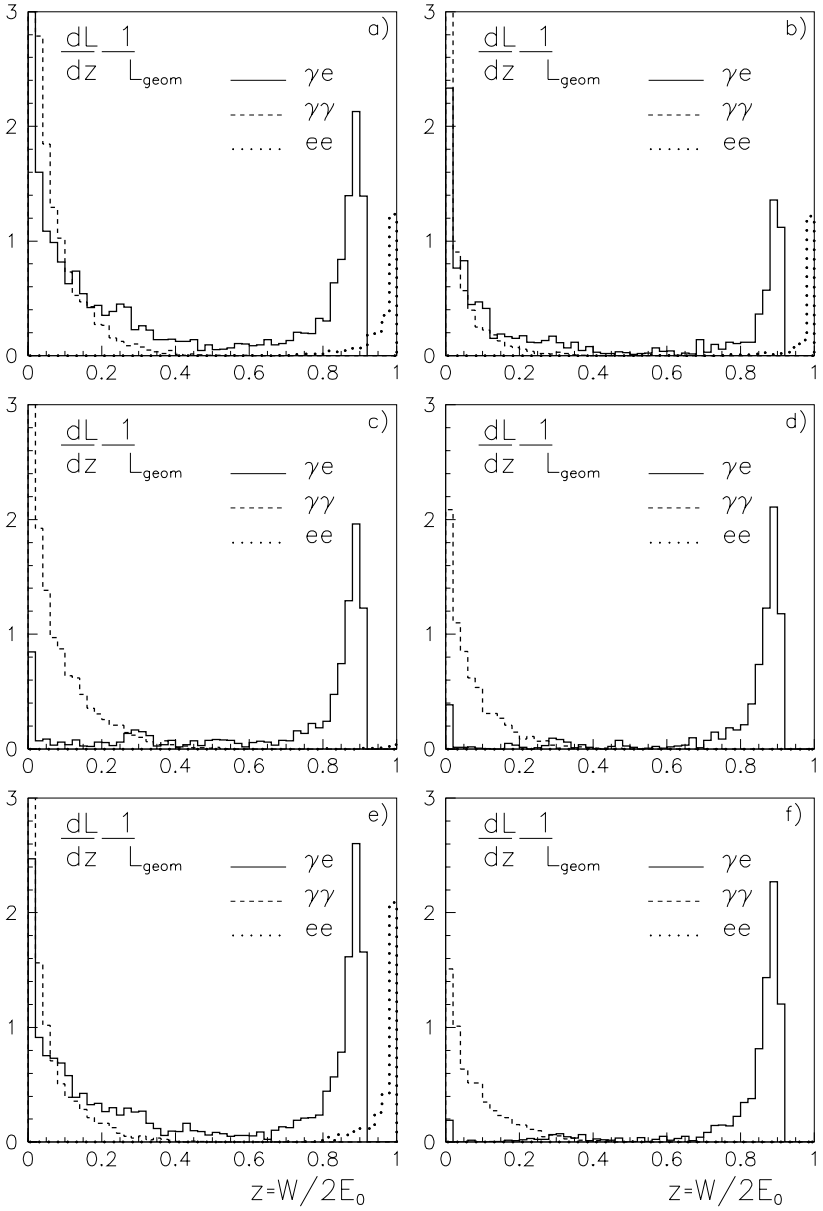

Figure A.12: *Spectral γe luminosity in the scheme with the horizontal deflection for beam parameters presented in Tables A.2, A.3. (Figs. A.12a), b)... correspond to TESLA(1), TESLA(2)...). For additional comments see the text.*

- The low energy γe and high energy ee luminosity in figs A.12 a), b), e) (cases with large σ_x) are connected with the collision of tails of the "main" electron beam with the swept electron beam. Likely it will not cause problems for the analysis. Further increase of b (length of the sweeping magnet) is not desirable, because

the transverse electron beam size at CP $\sigma_x(b) = \sigma_x(0)(b/\beta_x)$ will be comparable with the laser spot size and this leads to the decrease of the conversion coefficient.

We have seen that γe luminosity with optimized horizontal deflection is large enough and has good quality. Unfortunately this requires change of the sweeping magnet and some shift of optical elements. Therefore it was interesting to check what are γe luminosities when exactly the same deflection as for $\gamma\gamma$ case (vertical deflection) is used, but with one laser switched off and the "main" electron beam is somewhat shifted to collide with a high energy core of the γ-beam. The results for this case are presented in Fig. A.13 and Table A.3 (lane 5). We see that the high energy peak is lower and broader than with the horizontal deflection. This is mainly due to beam displacement in the field of the opposing beam. It is of interest that in some cases this displacement is much larger than σ_y and b/γ, but some luminosity at $z \sim z_{max}$ has survived. This is because the displacement during beam collisions grows quadratically with the passed distance and on the first part of collision length it is relatively small.

A.4.5.3 Ultimate luminosities

From the results presented in Table A.3 follows that $L_{\gamma\gamma}(z > 0.65)$ in the considered range of parameters is approximately proportional to the L_{geom} and the case TESLA(4) has maximum luminosity. What further improvement is possible providing the problem of low horizontal emittances is solved (laser cooling, for example)? Let us consider the case of TESLA(4) but with 5 times smaller emittances: $\epsilon_{xn} = \epsilon_{yn} = 2 \cdot 10^{-7}$ m·rad. The results are presented below and in Fig. A.14.

"Super TESLA(4)"

$N = 3.63 \cdot 10^{10}$, $\sigma_z = 0.5$ mm, $2E = 500$ GeV, $f = 5.65$ kHz,
$\epsilon_{nx} = \epsilon_{ny} = 0.2 \cdot 10^{-6}$ m· rad, $\beta_x = \beta_y = 0.5$ mm, $\sigma_x = \sigma_y = 14$ nm,
$L_{geom} = 2 \cdot 10^{35}$ cm^{-2} c^{-1}

no deflection: $b = \gamma\sigma_y = 0.7$ cm,

$L_{\gamma\gamma} = 1.15 \cdot 10^{35}$, $L_{\gamma\gamma}(z > 0.65) = 1.5 \cdot 10^{34}$ cm^{-2} c^{-1},
$L_{\gamma e} = 3.6 \cdot 10^{34}$, $L_{\gamma e}(z > 0.65) = 1.2 \cdot 10^{34}$ cm^{-2} c^{-1},
$L_{ee} = 1.5 \cdot 10^{32}$, $L_{ee}(z > 0.65) = 8 \cdot 10^{31}$ cm^{-2} c^{-1},
$L_{e^+e^-} = 6 \cdot 10^{32}$, $L_{e^+e^-}(z > 0.65) = 1.4 \cdot 10^{32}$ cm^{-2} c^{-1},
$L_{\gamma e^+} = 5.6 \cdot 10^{32}$, $L_{\gamma e^+}(z > 0.65) = 1.2 \cdot 10^{31}$ cm^{-2} c^{-1},

with magnetic deflection: $b = 1.5$ cm, $B = 0.5$ T,

$L_{\gamma\gamma} = 2 \cdot 10^{34}$, $L_{\gamma\gamma}(z > 0.65) = 1 \cdot 10^{34}$ cm^{-2} c^{-1},
$L_{\gamma e} = 2.5 \cdot 10^{33}$, $L_{\gamma e}(z > 0.65) = 6 \cdot 10^{32}$ cm^{-2} c^{-1},
$L_{ee} = 5 \cdot 10^{30}$ cm^{-2} c^{-1}

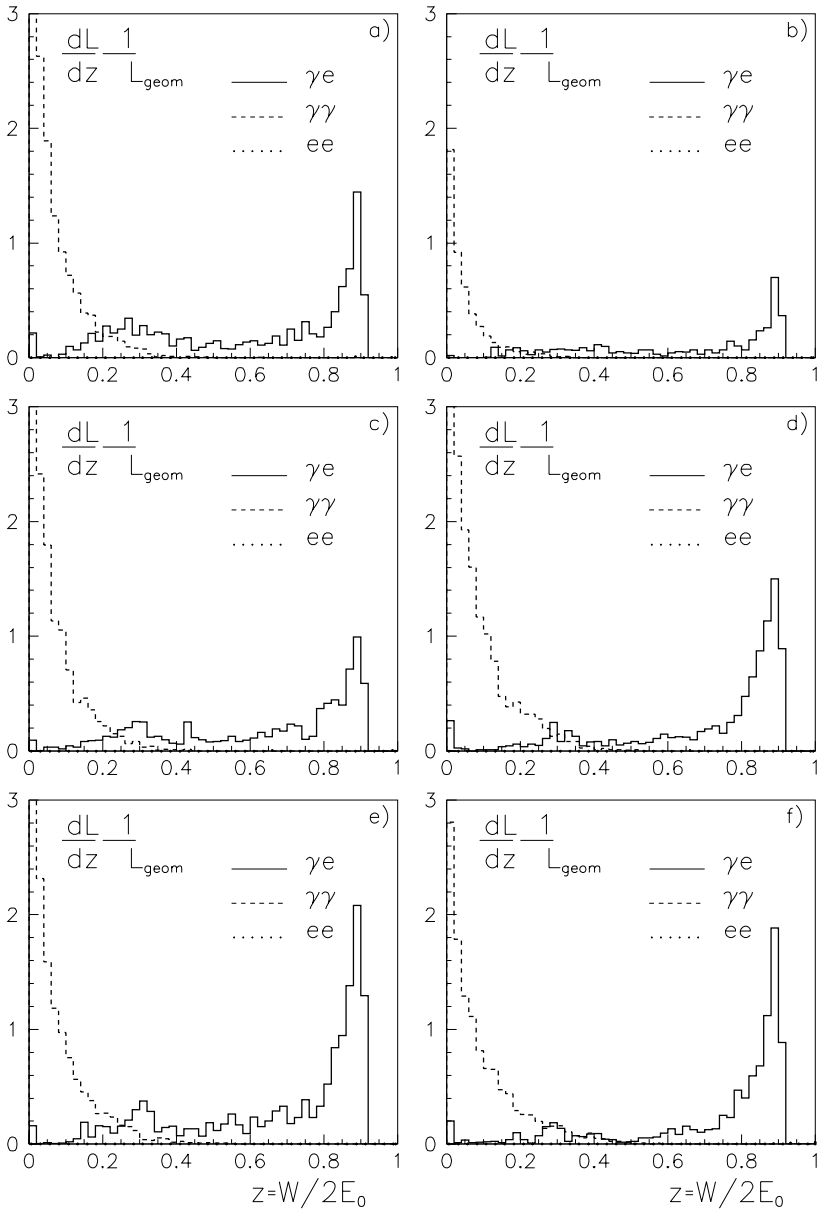

Figure A.13: *Spectral γe luminosity in the scheme with the same vertical deflection as for $\gamma\gamma$ collisions (fig. A.11) for beam parameters presented in Tables A.2, A.3. (Figs. A.13a), b)... correspond to TESLA(1), TESLA(2)...). For additional comments see the text.*

Results are impressive: $L_{\gamma\gamma}(z > 0.65) \geq 10^{34}$ cm^{-2}s^{-1} in both case with and without deflection. Let us note one interesting fact. The beams in this example have transverse sizes $\sigma_x = \sigma_y = 14$ nm and the parameter $\Upsilon \sim 3$, higher than the threshold of the coherent pair creation (see sect.4.2). In collisions without deflection we could

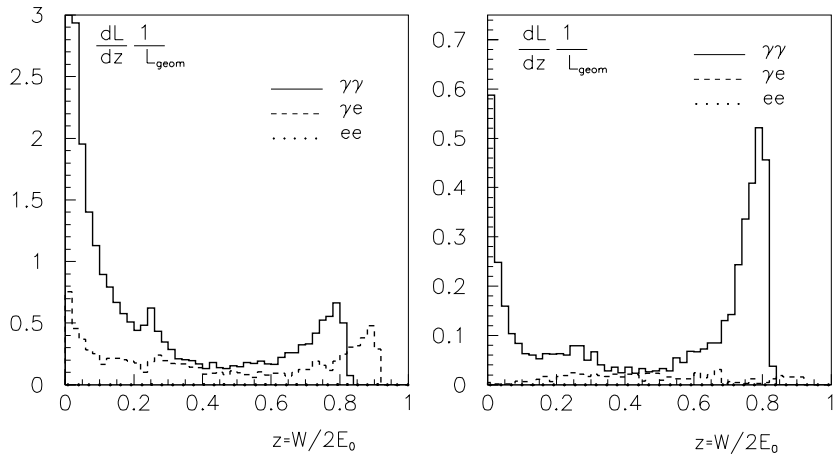

Figure A.14: *Luminosity spectra for the "super TESLA(4)" parameters (see the text). Left figure - without the deflection; right - $\gamma\gamma$ collisions with the magnetic deflection.*

expect very high conversion probability of the high energy photons to e^+e^- pairs. But simulation shows that there is no such problem, though there are some small e^+e^-, γe^+ luminosities. An explanation for this is the following[24]: due to repulsion beams are separated during the collision at a rather large distance and their field on the beam axis (which influence on high energy photons) is below the critical value $\Upsilon \sim 1$.

From this picture an incredible conclusion follows: one can use for $\gamma\gamma$ collisions the electron beams even with infinitely small transverse sizes (with N, σ_z, E_0 considered above)! The $\gamma\gamma$ luminosity will be determined by the photon spot size which is equal to b/γ. In this case [24]

$$L_{\gamma\gamma}(z > 0.65) \sim 0.35 \frac{k^2 N^2 f}{4\pi (b/\gamma)^2} \sim k^2 \left(\frac{N}{10^{10}}\right)^2 \frac{E^2[\text{TeV}\,] f[\text{kHz}]}{b^2[\text{mm}\,]} \cdot 10^{36} \qquad \text{(A.16)}$$

For TESLA with $b = 3$ mm, $k^2 = 0.4$ we get $L_{\gamma\gamma}(z > 0.65) \sim 2{\cdot}10^{35}$ cm^{-2}s^{-1}, providing $\sigma_x, \sigma_y \leq b/2\gamma = 3$ nm. The simulation confirms this result. The last example may sound too fantastic, but $L_{\gamma\gamma}(z > 0.65) \sim 10^{34}$ cm^{-2}s^{-1} demonstrated before (with and without magnetic deflection) is a good goal for "upgraded" TESLA (SBLC).

A.4.6 Summary table of $\gamma\gamma$,γe luminosities

The results on $\gamma\gamma$, γe luminosities collected on Table 3 and corresponding figures can be summarized as follows.

$\underline{\gamma\gamma\text{ -luminosities}}$

High energy $\gamma\gamma$ luminosity $L_{\gamma\gamma}(z \geq 0.65)$ is approximately the same in both collision schemes (with and without the deflection) and account for

Table A.3: *Possible parameters of the $\gamma\gamma$, γe collider. The cases of ultimate luminosities (sect. 4.5.3) are not included.*

	TESLA(1)	TESLA(2)	TESLA(3)	TESLA(4)	SBLC(1)	SBLC(2)
$N/10^{10}$	3.63	1.82	3.63	3.63	1.1	1.1
σ_z, mm	0.5	0.5	0.5	0.5	0.3	0.3
coll. rate, kHz	5.65	9.04	5.65	5.65	16.65	16.65
σ_x, nm	303	280	128	47	160	28
σ_y, nm	16	5.5	16	32	14	17.5
$L(geom), 10^{33}$	12.2	15.4	30.0	39	7.1	32.6
$\gamma\gamma$, no deflection, $b = 1.5\gamma\sigma_y$, see also Fig. A.10						
b, cm	1.17	0.41	1.17	2.35	1.04	1.28
$L_{\gamma\gamma}, 10^{33}$	13.2	11.	31.	34.	6.3	21.
$L_{\gamma\gamma}(z > 0.65)$	1.2	1.5	2.7	3.3	0.7	2.7
$L_{\gamma e}, 10^{33}$	8.7	7	17	22	5.9	16
$L_{\gamma e}(z > 0.65)$	2	2	4	5.5	1.6	5
$L_{ee}, 10^{33}$	0.86	0.6	0.72	1	1.05	1.15
$L_{ee}(z > 0.65)$	0.55	0.39	0.48	0.74	0.69	0.78
$\theta_x(\theta_y)_{max}, mrad$	6.5(7.5)	5.5(6)	6.5(9)	7.5(8)	4.5(6)	6(6)
$\gamma\gamma$, with vertical deflection, $B = 0.5$ T, see also Fig. A.11						
b, cm	1.5	1.5	1.5	2.35	1.5	1.53
$L_{\gamma\gamma}, 10^{33}$	4.9	2.2	10.2	8.2	2.3	6.2
$L_{\gamma\gamma}(z > 0.65)$	1.1	0.67	2.5	3.3	0.6	2.3
$L_{\gamma e}, 10^{33}$	1.0	0.47	1.65	1.0	0.67	1.6
$L_{\gamma e}(z > 0.65)$	0.16	0.01	0.25	0.14	0.1	0.45
$\theta_x(\theta_y)_{max}, mrad$	2.5(5)	2(4)	2.0(5.5)	0.5(3.5)	2(3)	1(2.3)
γe, with horizontal deflection, $B = 0.5$ T, see also Fig. A.12						
b, cm	3.5	3	3.5	4.5	3.0	2.5
$L_{\gamma e}, 10^{33}$	5.6	3.5	5.6	6.0	2.8	5.3
$L_{\gamma e}(z > 0.65)$	2	1.3	4.0	5.2	1.3	4.8
$L_{\gamma\gamma}, 10^{33}$	5.8	2.4	7.7	5.3	1.7	3.9
$L_{\gamma\gamma}(z > 0.65)$	< 0.001	< 0.001	< 0.001	< 0.001	< 0.001	< 0.001
$\theta_x(\theta_y)_{max}, mrad$	2.5(2.5)	2(2)	2(2.5)	2.5(2.5)	2(2)	2(2)
γe, with vertical deflection, optimized for $\gamma\gamma$, $B = 0.5$ T, see also Fig. A.13						
b, cm	1.5	1.5	1.5	2.35	1.5	1.53
$L_{\gamma e}, 10^{33}$	2.5	1.2	4.9	7.5	2.	6.
$L_{\gamma e}(z > 0.65)$	1.35	0.72	2.9	5.5	1.3	4.6
$L_{\gamma\gamma}, 10^{33}$	3.7	1.5	8.1	13	1.9	7.8
$L_{\gamma\gamma}(z > 0.65)$	< 0.001	< 0.001	< 0.001	< 0.001	< 0.001	< 0.001
$\theta_x(\theta_y)_{max}, mrad$	3(5.5)	2(3.5)	2.5(5.5)	2(6)	1(3)	2(2.5)

$L_{\gamma\gamma}(z \geq 0.65) \sim 10^{33}\mathrm{cm}^{-2}\mathrm{s}^{-1}$ for "nominal" (TESLA(1), SBLC(1)) parameters.
$L_{\gamma\gamma}(z \geq 0.65) \sim (1-3)\cdot 10^{33}\mathrm{cm}^{-2}\mathrm{s}^{-1}$ for beam parameters presented in Table 2 and in the top part of Table 3.

In the case of progress in obtaining electron beams with lower horizontal emittance one can get

$$L_{\gamma\gamma}(z \geq 0.65) \sim 10^{34} - 10^{35}\mathrm{cm}^{-2}\mathrm{s}^{-1}\ !$$

The peak luminosity is also an important characteristic. For all considered cases it is approximately

$$\frac{dL_{\gamma\gamma}}{dz} z_{max} \sim 7 L_{\gamma\gamma}(z > 0.65). \tag{A.17}$$

The ratio $L_{\gamma\gamma}(\mathrm{total})/L_{\gamma\gamma}(z \geq 0.65)$ is a less definite parameter, which depends on the distance between the CP and IP and on the value of the sweeping field (in the case with deflection). For considered variants, it changes between 2–4 and 8–11 for the schemes with and without deflection respectively. The hadronic background in the second case will be larger by a factor of 2 (see sect.5).

γe -luminosities

$L_{\gamma\gamma}(z \geq 0.65) \sim (1.5-5)\cdot 10^{33}\mathrm{cm}^{-2}\mathrm{s}^{-1}$ in both collision schemes. In the case with magnetic deflection the luminosity spectrum is quite monochromatic (FWHM$\sim$ 5%).

A priori it is clear that pure $\gamma\gamma$ and γe collisions with lower background in the scheme with deflection are simpler for analysis, but the scheme without deflection also has some positive features: no sweeping magnets, simultaneous $\gamma\gamma$, γe collisions, higher luminosity at low and intermediate invariant masses (they could be even higher with lower b). Further studies should show how serious the problems with analysis at these conditions are.

A.4.7 Monitoring and measurement of $\gamma\gamma$, γe luminosities

A system produced in a $\gamma\gamma$ collision is characterized by its invariant mass $\mathrm{W}_{\gamma\gamma} = \sqrt{4\omega_1\omega_2}$ and rapidity $\eta = 0.5\ln(\omega_1/\omega_2)$. We should have a method to measure 1) $d^2\mathrm{L}/d\mathrm{W}d\eta$ and 2)$\lambda_{\gamma 1}\lambda_{\gamma 2}$ or, in other words, $d\mathrm{L}_0/d\mathrm{W}d\eta$ and $d\mathrm{L}_2/d\mathrm{W}d\eta$ (0,2—total helicity of the system). This can be measured using the process $\gamma\gamma \to \mathrm{e}^+\mathrm{e}^-$ $(\mu^+\mu^-)$[16, 18].

For this process $\sigma_0/\sigma_2 \sim m^2/s$ (excluding the region of small angles), $s = 4E_0^2$. Therefore, the measurement of this process will give us $d\mathrm{L}_2/dzd\eta$. How to measure $d\mathrm{L}_0/dzd\eta$? This can be done by inversion of the helicity(λ_γ) of the one photon beam by means of changing simultaneously signs of helicities of the laser beam used for $\mathrm{e} \to \gamma$ conversion and that of the electron beam (in photo injector). In this case the spectrum of scattered photons is not changed while the product $\lambda_{\gamma 1}\lambda_{\gamma 2}$ changes its sign. In other words, what was before L_0 is now L_2, which we can measure. The cross section for this

process $\sigma(|\cos\Theta| < 0.9) \approx 10^{-36}/\mathrm{s}[\mathrm{TeV}^2]$, cm^2. This process is very easy to select due to a zero coplanarity angle.

Other processes with large cross sections which can be used for the luminosity measurement are $\gamma\gamma \to e^+e^-\ e^+e^-$ [2] and $\gamma\gamma \to W^+W^-$ [123]. The first process has the total cross section of $6.5 \cdot 10^{-30}$ cm^2, the second one $8 \cdot 10^{-35}$ cm^2. Unfortunalely, both these processes practically do not depend on the polarization and the first one is difficult for detection.

For the absolute γe luminosity measurement one can use the process of Compton scattering which is strongly polarization dependent.

For luminosity tuning one can use beam-beam deflection and background processes such as e^+e^- and hadron production. In the scheme without sweeping magnets the beam deflection method is sufficient. It is more difficult to control $\gamma\gamma$ collisions in the scheme with the magnetic deflection. Besides the process $\gamma\gamma \to hadrons$, there are other possibilities which were not yet studied, such as beam-beam deflection, e^+e^- production by a high energy photon in a collision with swept electrons (at large impact distances) or e^+e^- pair production in a collision with synchrotron photons from the sweeping magnet. Using the hadronic production as a "firm" signal of the $\gamma\gamma$ luminosity (hundreds events per train collision) one should continuously measure other collision characteristics enumerated above and use fast feedback (inside bunch train duration) to stabilize conditions when the hadron yield is maximum [124].

A.4.8 Sweeping magnet

Only few remarks on the sweeping magnet. It can be a thin one loop pulse magnet [122]. Considerations show that for $B = 0.5\ T$ there are now visible problems. Some arguments:

- This field produces a 1 atm pressure, for a few cm magnet this makes no problems.
- For 2 mm Al coil thickness and 3 cm magnet length the total average power is about 100 W for TESLA time structure and even less for SBLC.
- The thickness of the skin layer for Al alloy for $\nu \sim 0.25$ kHz is about 5 mm. Attenuation of the field by about 0.5 mm thick Al vacuum pipe will be small (can be compensated), may be some cooling of the vacuum chamber will be necessary. For SBLC (with 2 μs bunch train length) the duration of current pulses should be optimized taking into account this effect. With a dielectric vacuum pipe there will be no such problem.
- One loop pulse magnet contains no dielectric material and can be put (if necessary) inside the vacuum pipe.
- Contribution of multiple scattering at the magnet to the impact parameter resolution is about $\sigma = 30/P[\mathrm{GeV}]$, μm for $\vartheta = \pi/2$, which is acceptable.

A.5 Backgrounds

What are backgrounds at $\gamma\gamma$,γe collider? Are they larger or smaller than in e^+e^- collisions? Let us try to answer these questions.

At $\gamma\gamma$,γe colliders there are following sources of backgrounds:

a) particles with large disruption angles hitting the final quads. The sources are multiple Compton scattering, hard beamstrahlung, Bremsstrahlung (in ee).

b) e^+e^- pairs created in the processes of ee $\to$ eee^+e^- (Landau-Lifshitz, LL), γe $\to$ ee^+e^- (Bethe-Heitler, BH), $\gamma\gamma \to e^+e^-$ (Breit-Wheeler, BW). This is the main source of low energy particles, which can cause problems in the vertex detector.

c) $\gamma\gamma \to hadrons$, $\gamma\gamma \to e^+e^-e^+e^-$ — the processes with largest cross-sections in $\gamma\gamma$ collisions.

We have already discussed the item a) before and found that the minimum energy of these particles is about 2% of E_0, the maximum disruption angle is below 10 mrad and they can be removed using the crab crossing scheme.

The Bremsstrahlung process $e^+e^- \to ee\gamma$ is suppressed at photon colliders (due to beam repulsion or magnetic deflection). In the scheme without deflection L_{ee}/crossing $\sim 10^{33}/10^4 = 10^{29}$ cm^{-2}s^{-1} per beam crossing. The low energy electrons after hard bremsstrahlung can have an energy below 2% E_0 and therefore hit the quads. The total energy of these particles for L_{ee} given above is about $1.5E_0$ per bunch crossing, which is small.

The item b) for γe, $\gamma\gamma$ colliders is even less important than for e^+e^- colliders because one of the main sources (LL) is almost absent. Nevertheless, we will consider here main characteristics of e^+e^- pairs which are important for designing sweeping magnets (aperture) and vacuum chamber near the IP.

Most of e^- and e^+ produced in LL, BH, BW processes travel in a forward direction, but due to the kick in the field of the opposing electron beam they get much larger angles and can cause problems in the detector. We have simulated these processes for two situations: 1) TESLA(1) without deflection (see Fig. A.10a) and Table A.3), 2) TESLA(1) with magnetic deflection (see Fig. A.11a). The total number of e^+e^- pairs produced in these cases per one bunch collision is 46000 and 7000 respectively. The distributions are presented in Fig. A.15. In the plot $p_\perp$ vs ϑ we see two regions of points concentration. The region with large $p_\perp$ corresponds to electrons deflected off the opposing beam (it was assumed in the simulation that e^+ have no kick). In the second case (with deflection) the backgrounds are much smaller.

Any materials near the IP should be located beyond the zone occupied by kicked particles. The background due to the particles with large initial angles is rather small. The shape of the zone occupied by the kicked electrons is described by the formula [125]

$$r^2_{max} \simeq \frac{25Ne}{\sigma_z B} z \sim 0.12 \frac{N}{10^{10}} \frac{z[\mathrm{cm}]}{\sigma_z[\mathrm{mm}]B[\mathrm{T}]} \qquad \text{(A.18)}$$

where r is the radius of the envelope at a distance z from the IP, B is longitudinal detector field. For example, for TESLA ($N = 3.63 \cdot 10^{10}, \sigma_z = 0.5$ mm, $B = 3$ T) $r = 0.55\sqrt{z[\mathrm{cm}]}$, cm. This simple formula can be used for the choice of a vertex

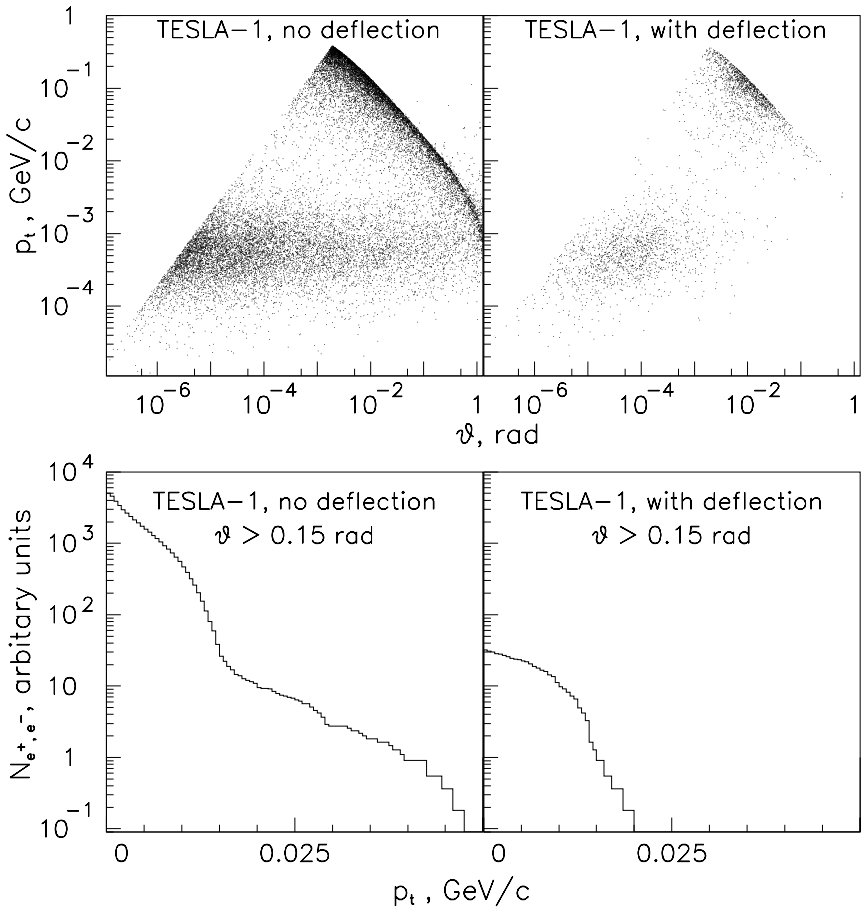

Figure A.15: *Upper figures: scatter plots of transverse momentum vs azimuthal angle, lower figures: $p_\perp$ distribution of e^+e^- with $\theta \geq 0.15$ rad.*

detector radius and aperture of the sweeping magnet. At $z = b \simeq 3$ cm (sweeping magnet) we have $r \simeq 0.95$, cm. For the cylindrical vertex detector with $l = \pm 15$ cm $r = 2.15$ cm.

Note that the sweeping magnet (with transverse field) gives to all particles $p_\perp = eB_e l/c$, where l is CP–IP distance. For $B_e = 0.5$ T and $l = 2$ cm $p_\perp = 3$ MeV/c. The spiral radius for these electrons in 3 T field is 0.33 cm. This is not dangerous, but larger B_e could make problems. This is very important point restricting the value of field in the sweeping magnet.

The total energy of all e^+e^- produced in the considered processes per one beam collision is $1.6 \cdot 10^6$ GeV and $1.7 \cdot 10^5$ GeV respectively for the cases TESLA(1, without deflection) and TESLA(1, with deflection). But most of these particles escape the detector inside a 10 mrad cone without interaction, and only particles with $\vartheta > 10$ mrad and $p \lesssim 1$ GeV (due to crab crossing in the solenoidal field) will hit the quads. The total energy of these particles is much smaller: $2 \cdot 10^4$ and $0.5 \cdot 10^4$ GeV for the two cases respectively. The conical mask (the same as for e^+e^- collision) around the beam can protect the detector from the low energy backscattered particles from electromagnetic

showers.

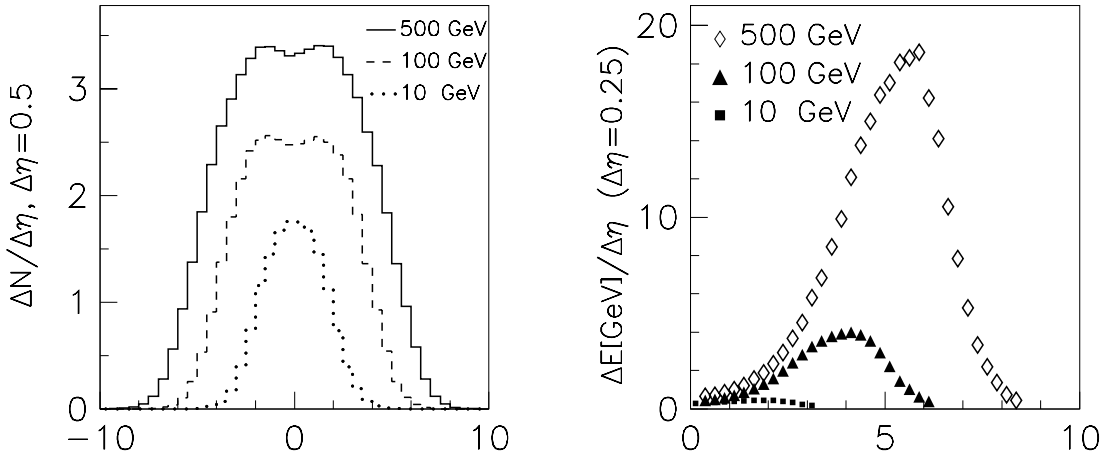

Figure A.16: *Distribution of particles (left) and energy flow (right) on pseudorapidity in $\gamma\gamma \to$ hadrons events (photons have equal energies).*

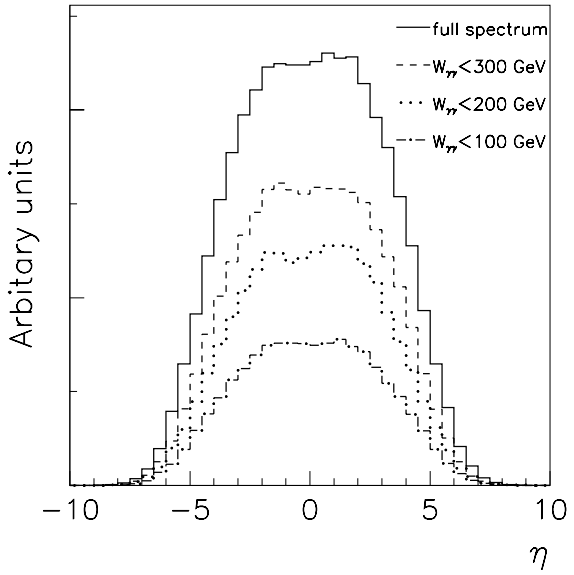

Figure A.17: *Distribution of particles on pseudorapidity for different ranges of $\gamma\gamma$ invariant mass for the TESLA(1) case without the deflection (see Fig. A.10a).*

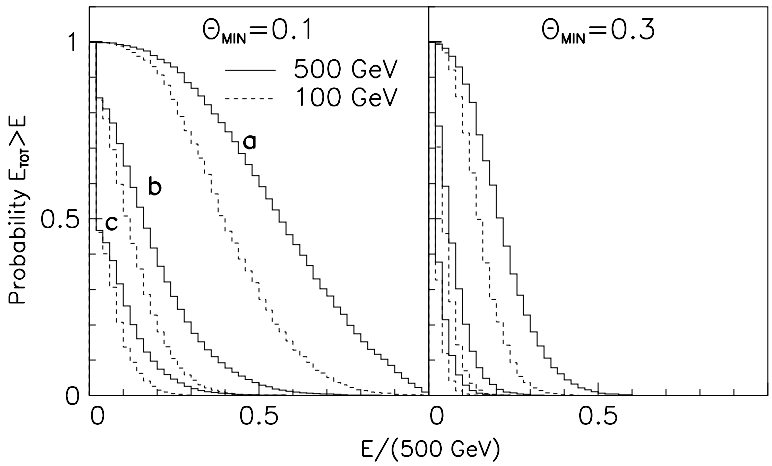

Figure A.18: *Probability of energy deposition in the detector above some value (E/500 GeV) due to the process $\gamma\gamma \to$ hadrons. The polar angle acceptance is $\vartheta > 0.1$ rad (left plot) and $\vartheta > 0.3$ rad (right plot). Curves a), b), c) correspond to 7, 2 and 0.7 hadronic events in average per beam collision respectively. The collision energy is 500 GeV (solid line) and 100 GeV (dashed line), photons have equal energies.*

The item c) $\gamma\gamma \to$ *hadrons* is the most specific background for a photon collider. The cross section of this process is about $400 - 600$ nb at $2E = 10 - 500$ GeV. The $\gamma\gamma$ luminosity is $2{\cdot}10^{29} - 5{\cdot}10^{30}$ cm^{-2}s^{-1} per bunch crossing (see Table A.3), which leads to $0.1 - 2.5$ events per beam collision. We considered also the cases of "superluminosities" which have even more events per crossing. What does it mean for experiment and where is the limit? To understand this we have performed simulation using the PYTHIA code 5.720 [126]. Fig. A.16 shows the distributions of particles and energy on pseudorapidity ($\eta = -\ln\tan(\vartheta/2)$) in one $\gamma\gamma \to$ *hadrons* event at $2E = 10, 100$ and 500 GeV. We see that each 500 GeV hadronic event gives on the average 25 particles (neutral + charged) in the range of $-2 \leq \eta \leq 2$ ($\vartheta \geq 0.27$ rad) with the total energy about 15 GeV. The average momentum of particles is about 0.4 GeV. Note that the flux of particles at large angles ($\eta = 0$) from 10 GeV event is only twice smaller than that from a 500 GeV $\gamma\gamma$ collision.

In this respect it is of interest to check what background gives different parts of $\gamma\gamma$ luminosity spectra for the scheme without deflection. Fig. A.17 also shows the distribution of particles on pseudorapidity for the TESLA(1) case. We see that the suppression of $\gamma\gamma$ luminosity in the region of $W_{\gamma\gamma} \leq 200$ GeV using the magnetic deflection decreases the hadronic backgrounds by a factor of two.

The probability of energy deposition in the detector above some value (E/500 GeV) is shown in Fig. A.18. In the left figure the minimum angle of the detector is 0.1 rad, on the right one 0.3 rad. Curves a), b), c) correspond to 7, 2 and 0.7 hadronic events on the average per collision; solid curves are for $2E = 500$ GeV, dashed are for 100 GeV. For 7 events per collision and $\vartheta_{min} = 0.1$ the energy deposition in the detector with 50% probability exceeds 55% of $2E_0$. But this energy is produced by about 300 rather soft particles. This smooth background can be subtracted. More important are

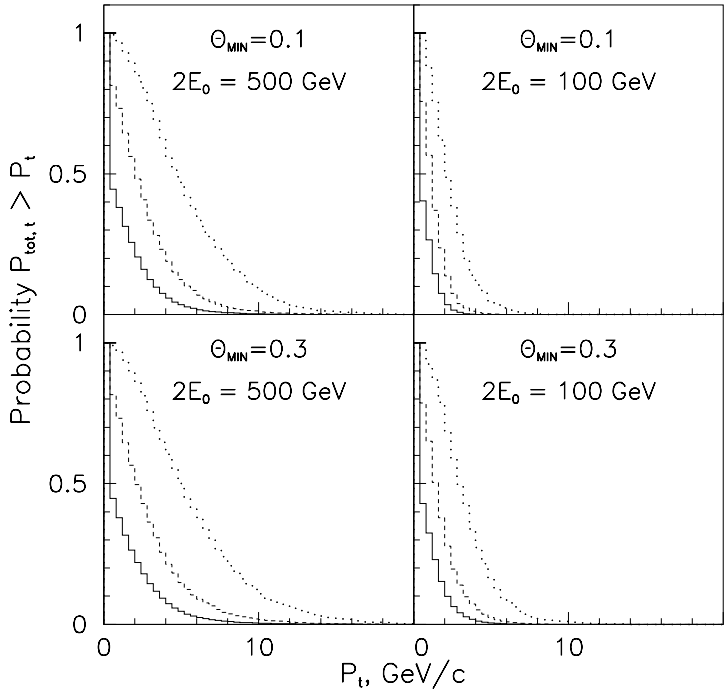

Figure A.19: *Probability to find an unbalanced transverse momentum above some p_t. Dotted, dashed and solid curves correspond to 7, 2, 0.7 $\gamma\gamma \to$ hadrons events in average per beam collision. The polar angle acceptance is $\vartheta > 0.1$ rad (upper plots) and $\vartheta > 0.3$ rad (lower plots). The collision energy is 500 GeV (left plots) and 100 GeV (right plots), photons have equal energies.*

the fluctuations of background. Below there are some of such characteristics.

In many experiments the important characteristic is a missing transverse momentum. The probability to find an unbalanced transverse momentum above some p_t is shown in Fig. A.19 for $\vartheta_{min} = 0.1$ and 0.3, for 500 and 100 GeV $\gamma\gamma$ collisions. Again 3 curves in each figure correspond to 7, 2, 0.7 hadronic events on the average per collision. The results are interesting. Comparing the curves at $\vartheta_{min} = 0.1$ and $\vartheta_{min} = 0.3$ we see that the difference is small, which is surprising because in the second case the energy deposition in the detector is by a factor of 2.6 smaller. The explanation is the following: in the second case the detector measures smaller part of the total energy and the fluctuations are larger (at $\vartheta_{min} = 0$ all particles are detected and in a perfect detector unbalanced $p_\perp = 0$). Let us look at the numbers. Even with 7 events (500 GeV) per collision the probability to get unbalanced $p_\perp \geq 10$ GeV is only about 10%, which is almost acceptable.

While calculating $p_\perp$, we summed all energy depositions in the detector, but "interesting" events usually have high energetic particles or jets. Let us check what the probability that the hadronic background adds some additional energy to a jet. This information is presented in Fig. A.20. We have selected a cell $\Delta\varphi \leq 0.3$, $\Delta\eta \leq 0.3$,

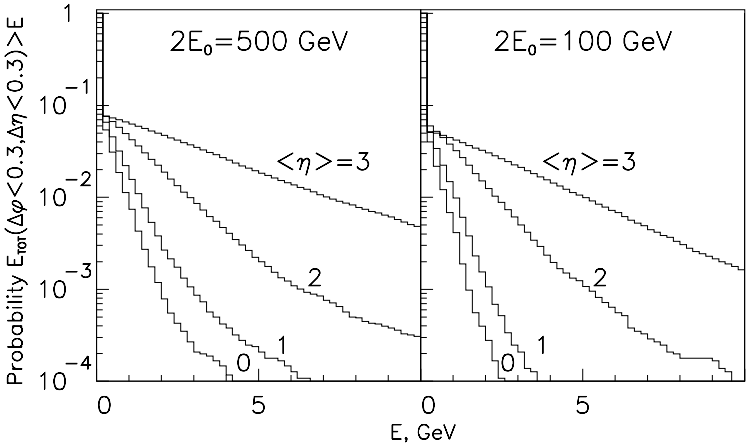

Figure A.20: *Probability to have the energy flow into* $\Delta\phi \times \Delta\eta = 0.3 \times 0.3$ *cell above some threshold (abscissa value) for 4 pseudorapidity points:* $\eta = 0$*, 1, 2, 3. The energy of symmetrical* $\gamma\gamma$ *is 500 GeV (left) and 100 GeV (right).*

which corresponds to a characteristic jet transverse size, and calculated the probability of energy deposition in this region above some energy E. The curves correspond to one hadronic event on the average per bunch collision. For other levels of background the probability should be multiplied by the average number of hadronic events per collision. A typical energy resolution for 100 GeV jet is about 4 GeV. The probability to have such energy deposition at $\eta = 0$ and 10 events per collision is less than 0.1%, at $\eta = 2$ ($\vartheta = 0.27$ rad) it is 4%, which is acceptable. Note that the average number of background particles in $\Delta\varphi \times \Delta\eta = 0.3 \times 0.3$ cell for a 500 GeV $\gamma\gamma$ collision is $\sim 0.1 \cdot n_{ev/coll}$, so for $n \leq 10$ the energy depostion (which we used) and its r.m.s. fluctuations are close to each other.

So, we can conclude that even 10 hadronic events in a 500 GeV $\gamma\gamma$ collision are acceptable for experiments. In the central part of the detector ($\eta \leq 1$,$\Delta\Omega/4\pi = 0.76$) even 50 events per collision lead to only 5% probability that background shifts the jet energy by one r.m.s. energy resolution. This condition corresponds at TESLA to $L_{\gamma\gamma} = 5 \cdot 10^{35}$ cm^{-2}s^{-1}.

A.6 Optics in the interaction region.

In this section it is considered how to bring laser beam into and out of CP. Our solution is shown in Fig. A.21. What is essential here.

1) It is attractive to place the focusing mirror out of the incoming and outgoing electron beams. Unfortunately in this case the required laser flash energy should be larger by a factor of 3 (the dependence of the flash energy on the angle between the laser and electron beam is shown in fig. A.22 for flattop and Gaussian beams). Therefore we have chosen the head-on collision. In this case each of focusing mirrors have two holes for the incoming and outgoing beams.

2) The opening angles of the final mirror M2 is dictated by the optimum laser

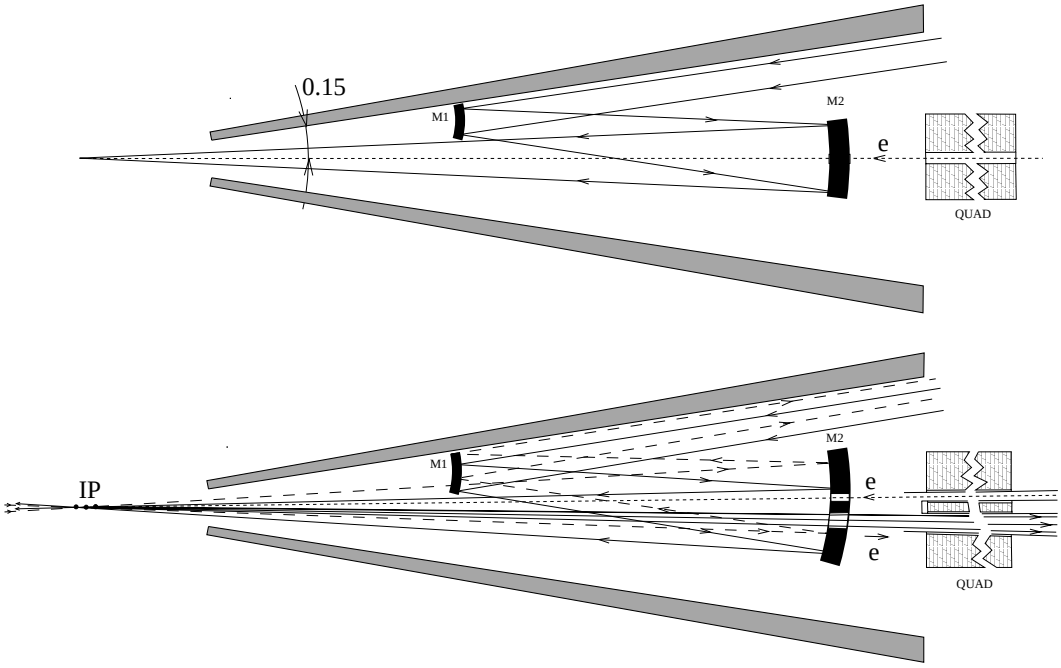

Figure A.21: *Layout of laser optics near the IP; upper - side view, down - top view, dashed lines - exit path of light coming from the left through one of the CP points (right to the IP), see comments in the text.*

divergence at the CP. The calculations are performed in section 3. The minimum distance between the M2 mirror and IP is determined by the mirror damage threshold. For $A = 3$ J, $\alpha_{\gamma,x} = 0.018$ (for $Z_R = 0.25$ mm, $\lambda = 1\mu$m) it would be sufficient to take this distance ~ 85 cm. In this case the fluence is 0.2 J/cm^2, while the damage threshold is in the 0.7-2 J/cm range [31, 127]. However, we put the focusing mirror M2 at a much larger distance (180 cm) to provide near normal incidence of the incoming laser beam (for smaller aberrations). Laser pulse comes to M2 after a second slightly defocusing mirror M1 placed between the IP and M2. In the case of using a plate mirror at the M1 location the larger opening angle of the shielding mask is required. The diameter of the focusing mirror M2 is about 20 cm ($\sim 3\alpha_{\gamma,x}$) and that of M1 is twice smaller.

3) Due to the crab crossing angle $\alpha_c = 30$ mrad (see Fig.7) the horizontal size of focusing mirrors is somewhat larger than the vertical one to provide the exit pass of the opposing laser beam. As soon as the distance between two CP points is small, the incoming and outgoing laser beams are practically parallel, but somewhat shifted.

The scheme shown in Fig. A.21 describes the case of head-on collisions of the laser and electron beams. Due to crab crossing collisions of the electron beam it is advantageous to have crab crossing of the laser-electron beam collision too (it was explained in sec.3). Fig. A.21 is valid for this option after some shift of the mirrors.

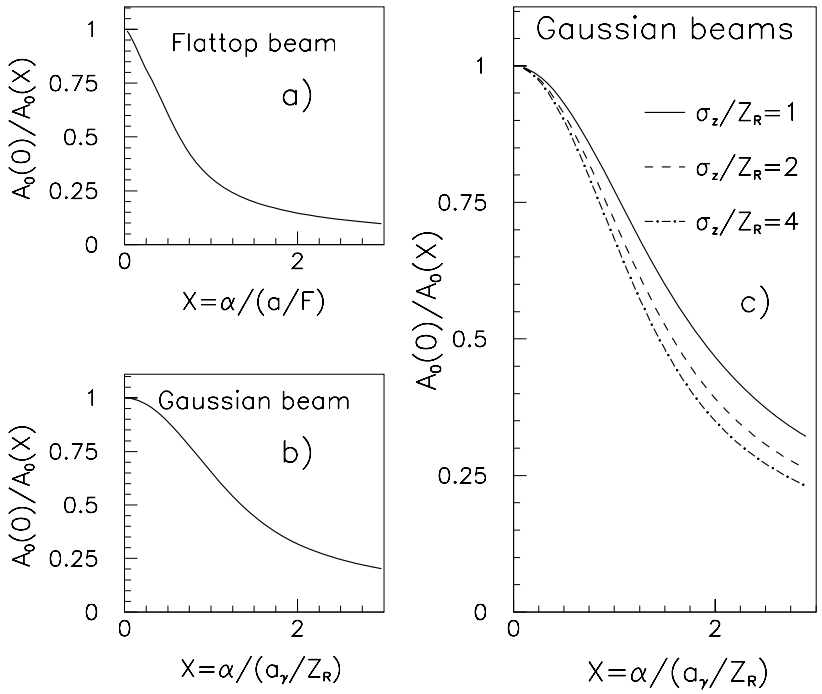

Figure A.22: *Dependence of the required laser flash energy on the collision angle between the laser and electron beams; (a) flattop, (b) Gaussian beams. Plots a), b) correspond to very long laser beams. Plot c) shows the same for Gaussian beams for different ratios of* σ_z/Z_R *assuming that* $\sigma_{L,z} = \sigma_z$.

A.7 Lasers

From section 3 follows that for obtaining the conversion probability $k \sim 65\%$ at $x = 4.8$ and $E_0 = 250$ GeV a laser with the following parameters is required:

Power	$P \sim 0.7$ TW
Duration	$\tau(rms) \sim \sigma_z/c \sim 1 - 2.5$ ps
Flash energy	2 - 4 J
Repetition rate	collision rate at a collider
Average power	~ 25 kW
Wave length	$\lambda = 4.2E_0$[TeV], μm

Obtaining of such parameters is possible with solid state or free electron lasers (FEL). For $\lambda \geq 1\mu$m ($E_0 \gtrsim 250$ GeV) FEL is the only option seen now.

A.7.1 Solid state lasers

The region of $\lambda \sim 1$ μm is convenient for solid state lasers, namely this is a wave length of the most powerful Nd:Glass lasers. In the last 10 years the technique of short

powerful lasers made an impressive step and has reached petowatt (10^{15}) power levels and few femtosecond durations [128]. Obtaining few joule pulses of picosecond duration is not a problem for a modern laser technique. For photon collider applications the main problem is a high repetition rate. This is connected with overheating of the media.

The success in obtaining picosecond pulses is connected with a chirped pulse amplification (CPA) technique [129]. "Chirped" means that the pulse has a time-frequency correlation. The main problem in obtaining short pulses is the limitation on peak power imposed by the nonlinear refractive index. This limit on intensity is about 1 GW/cm^2. CPA technique succesfully overcomes this limit.

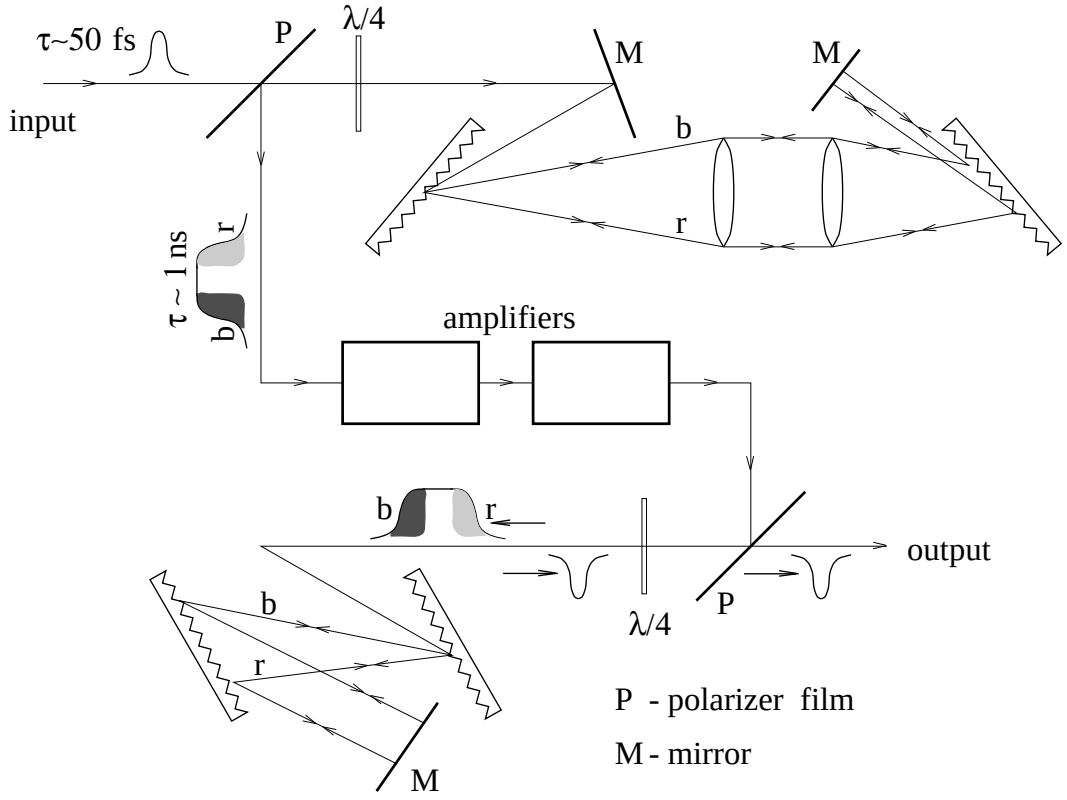

Figure A.23: *Chirped pulse amplification.*

The principle of CPA is demonstrated in Fig. A.23. A short, low energy pulse is generated in an oscillator. Then this pulse is stretched by a factor about 10^4 in the grating pair which has delay proportional to the frequency. This long nanosecond pulse is amplified and compressed by another grating pair to a pulse with the initial or somewhat longer duration. Due to practical absence of non-linear effects, the obtained pulses have a very good quality close to the diffraction limit.

One of such lasers [130] works now in the E-144 experiment studing nonlinear QED effects in the collision of laser photons and 50 GeV electrons. It has a repetition rate of 0.5 Hz, $\lambda = 1.06$ μm (Nd:Glass), 2J flash energy, 2 TW power and 1 ps duration.

This is a top-table laser. Its parameters are very close to our needs, only the repetition rate is too low.

In this laser a flashlamp pumping is used. Further progress in the repetition rate (by two orders) is possible with a diode pumping (high efficiency semiconductor lasers). This technology is fast developing and promoted by other big projects. With diode pumping the efficiency of solid state lasers reaches a 10% level. Recent studies [131, 132, 31] have shown that the combination of CPA, diode pumping, recombining of several lasers (using polarizers and Pockel cells or slightly different wave lengths), and (if necessary) other laser techniques such as phase-conjugated mirrors, moving amplifiers allows already now to build a solid state laser system for a photon collider.

All necessary technologies are developing actively now for other (than HEP) applications. The detailed design of the solid state laser system for the $\gamma\gamma$, γe colliders requires special R&D study.

A.7.2 Free Electron Lasers

Potential features of a free electron laser (FEL) allow one to consider it as an ideal source of primary photons for a gamma-gamma collider. Indeed, FEL radiation is tunable and has always minimal (i.e. diffraction) dispersion. The FEL radiation is completely polarized: circularly or linearly for the case of helical or planar undulator, respectively. A driving accelerator for the FEL may be a modification of the main linear accelerator, thus providing the required time structure of laser pulses. The problem of synchronization of the laser and electron bunches at the conversion region is solved by means of traditional methods used in accelerator techniques. A FEL amplifier has potential to provide high conversion efficiency of the kinetic energy of the electron beam into coherent radiation. At sufficient peak power of the driving electron beam the peak power of the FEL radiation could reach the required TW level.

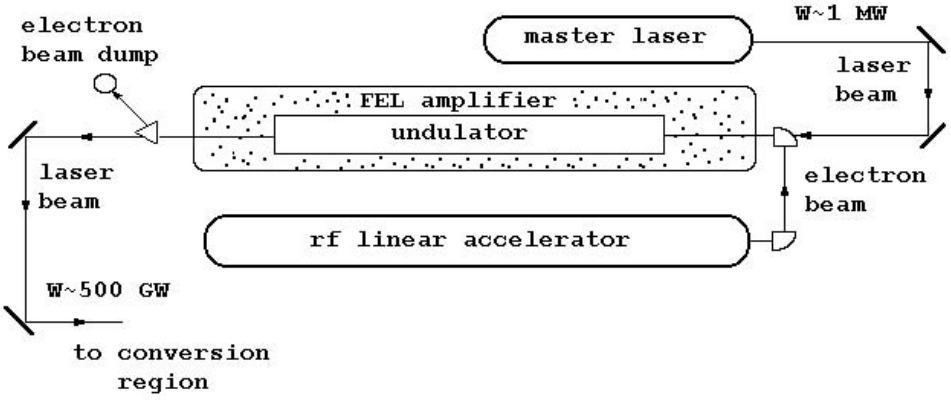

Figure A.24: *MOPA FEL configuration for a gamma-gamma collider.*

The idea to use a FEL as a laser for the gamma-gamma collider has been proposed in ref. [8]. A more detailed study of this idea has shown that the problem of construction

of free electron laser can be solved using Master Oscillator – Power Amplifier (MOPA) scheme with the driving accelerator for the FEL amplifier constructed on the same basis as the main accelerator for a linear collider [133, 134, 135, 136]. At present an option of FEL as a laser for the gamma-gamma collider is studied for different projects. While there exist different FEL configurations, an amplifier configuration has definite advantages for application in the gamma-gamma collider schemes [136]. The choice of specific technical solution depends on the parameters of the linear collider project. For instance, for the VLEPP, CLIC, JLC and TESLA projects it has been considered to use MOPA FEL scheme [137, 138, 20, 141, 142]. Designers of NLC project consider a FEL scheme using an induction linac and chirped pulse amplification technique [143, 144].

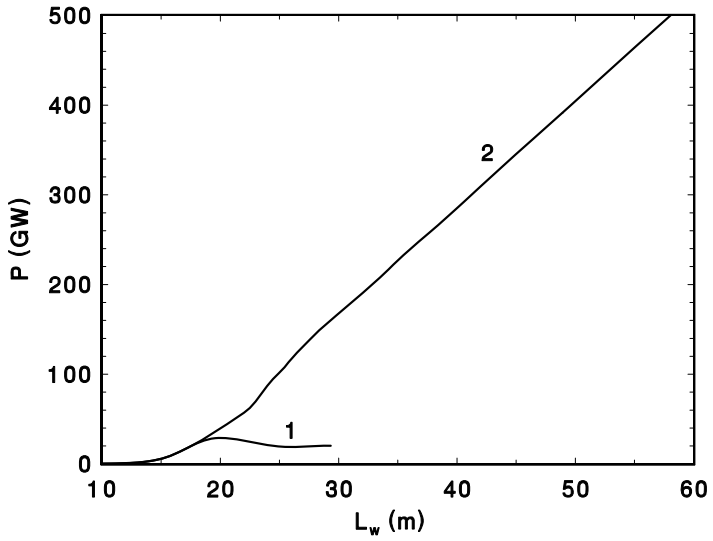

Figure A.25: *Output power of the FEL amplifier versus undulator length.*

In the present study of the Linear Collider Project it has been accepted to use MOPA FEL scheme as a laser (see Fig. A.24). Such a choice fits well to both TESLA and SBLC options. In this scheme the optical pulse from Nd glass laser ($\lambda = 1$ μm, 1 MW peak power) is amplified by the FEL amplifier up to the power of about 500 GW (see Table A.4). The driving beam for the FEL amplifier is produced by the linear rf accelerator identical to the main accelerator, but with lower accelerating gradient due to the higher beam load. It is important that the requirements to the parameters of the FEL driving electron beam are rather moderate and can be provided by an injector consisting of gridded thermoionic gun and subharmonic buncher.

Table A.4 presents the main parameters of the FEL amplifier and the driving accelerator. It is seen from Fig. A.25 that 500 GW level of output power is achieved at the undulator length of about 60 m. The total flash energy in the laser pulse is about of 2 J.

Using the FEL amplifier allows one to completely exclude transmitting optical

Table A.4: *Parameters of the FEL amplifier*

Electron beam*	
Electron energy	2 GeV
Peak beam current	2.5 kA
rms energy spread	0.2 %
rms normalized emittance	$2\pi \times 10^{-2}$ cm rad
rms bunch length	1 mm
Undulator	
Undulator type	Helical
Undulator period (entr.)	15 cm
Undulator field (entr.)	10.2 kG
External β-function	2 m
Length of untapered section	17 m
Total undulator length	60 m
Radiation	
Radiation wavelength	1 μm
Input power	1 MW
Output power	500 GW
Flash energy	2.3 J
Efficiency	10 %

*Time diagram of the accelerator operation is identical to the time diagram of the main accelerator.

elements and deliver the laser beam to the conversion region using several reflections from metallic mirrors which are rather stable to the laser radiation damage. This can be done when vacuum systems of the FEL amplifier and linear collider are combined. The first reflection mirror can be installed at a distance about several tens of meters after the exit of the undulator when the laser beam expands to the size about several centimeters.

To reduce the cost of laser system, only one free electron laser can be used. This scheme operates as follows. The FEL is installed only in one branch of the linear collider. When the laser bunch passes the focus of the conversion region, it is not dumped but is directed to the optical delay line which provides a delay time equal to the time interval between the bunches. Then it is focused on the electron beam of the opposite branch of the linear collider. Of course, this configuration provides colliding gamma-beams with the second micropulse of the collider. Nevertheless, the number of microbunches is equal to several hundreds, so it will not result in significant reduction of the integral luminosity.

A.7.2.1 Future perspectives

The present design has been limited with an approach which can be realized at the present level of accelerator and FEL technique. The main reserve to improve the FEL

performance is to increase its efficiency which will allow to decrease the requirements to the value of the peak electron beam power. The perspectives of the FEL efficiency increase are on the way of using multi-stage FEL amplifier with diaphragm focusing line (see Fig. A.26) [145, 20]. The principle of operation of this FEL scheme consists in the storing of the energy in a single laser pulse amplified by a sequence of electron bunches. This scheme has evident perspectives for the TESLA project due to a large bunch spacing. Preliminary study shows that the energy of the driving electron beam could be reduced to the value of several hundreds of MeV and the value of the peak current could be reduced by several times. The beam load in accelerator will be also reduced approximately by a factor of 3 due to higher FEL efficiency about of 30 %.

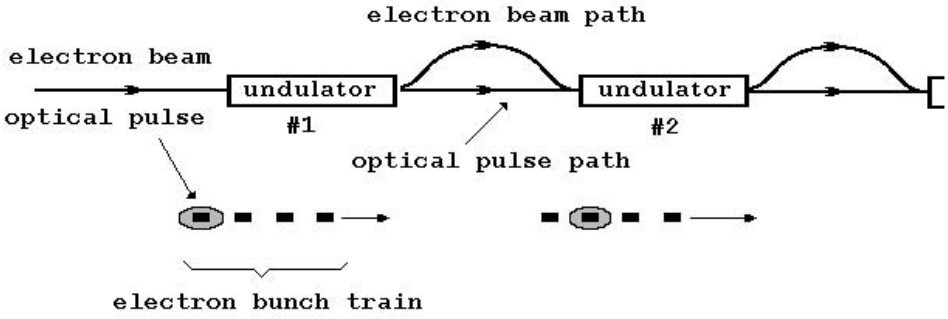

Figure A.26: *The scheme of multi-stage FEL amplifier. One optical pulse is amplified by a sequence of electron bunches. The peak power of the output radiation exceeds by a factor of N (number of amplification stages) the peak output radiation power of traditional single pass FEL amplifier.*

Bibliography

[1] I.Ginzburg,G.Kotkin,V.Serbo,V.Telnov,*Pizma ZhETF*, **34** (1981)514; *JETP Lett.* **34** (1982)491; (*Prep.INF* 81-50,Novosibirsk, Feb.1981,in english).

[2] I.Ginzburg, G.Kotkin, V.Serbo, V.Telnov, *Nucl.Instr. & Meth.* **205** (1983) 47.

[3] I.Ginzburg, G.Kotkin, S.Panfil, V.Serbo, V.Telnov, *Nucl. Instr. & Meth.* **219** (1984)5.

[4] V.Telnov,*Nucl.Instr.&Meth.* **A294** (1990)72.

[5] V.Telnov, *Proc.of Workshop on Gamma-Gamma Colliders,* Berkeley CA, USA, 1994, *Nucl.Instr.&Meth.* **A355**(1995)3.

[6] V.Balakin,A.Skrinsky,*Prep.INF* 81-129,Novosibirsk, 1981.

[7] A.Skrinsky, *Uspekhi Fiz.Nauk* **138** (1982) 3.

[8] A.Kondratenko,E.Pakhtusova,E.Saldin, *Dokl.Akad.Nauk*, **264**(1982)849.

[9] J.Spencer, SLAC-PUB-3645, 1985

[10] J.Sens, *Proc.of* 8^{th} *Int.Workshop on Photon-Photon Collisions*, Israel, Apr. 1988.

[11] P.Chen,V.Telnov,*Phys.Rev.Letters*, **63** (1989)1796.

[12] V.Telnov,*Proc.of Workshop on Phys. and Exper. with Linear Colliders,* Sept.9-14, 1991, Lapland, Finland.

[13] V.Telnov,*Proc. of IX Intern. Workshop on Photon-Photon collisions*, San Diego 1992, World Scientific

[14] D.Borden,D.Bauer,D.Caldwell, *SLAC-PUB*-5715, *UCSD-HEP*-92-01.

[15] D.L.Borden, *Proc.of Workshop on Physics and Exper.with Linear* e^+e^- *Colliders*, Waikoloa, Hawaii, Apr.1993, World Scientific, 1993, p.323.

[16] V.Telnov, *Proc.of Workshop on Physics and Exper.with Linear* e^+e^- *Colliders*, Waikoloa, Hawaii, Apr.1993, World Scientific, 1993, p.323.

[17] F.Richard, *Proc.of Workshop on Gamma-Gamma Colliders,* Berkeley CA, USA, 1994, *Nucl.Instr.&Meth.* **A355**(1995)92.

[18] D.Miller, *Proc.of Workshop on Gamma-Gamma Colliders,* Berkeley CA, USA, 1994, *Nucl.Instr.&Meth.* **A355**(1995)101.

[19] V.Balakin, A.Sery, *Proc.of Workshop on Gamma-Gamma Colliders,* Berkeley CA, USA, 1994,*Nucl.Instr.&Meth.A* **355**(1995)157.

[20] E.Saldin, V.Satantsev, E.Scneidmiller, Yu.Ulyanov, M.Yurkov *Nucl. Instr. &Meth.* **A355**(1995)171; **A361**(1995)101; **A361**(1995)317.

[21] J.Spencer, *Proc.of Workshop on Gamma-Gamma Colliders,* Berkeley CA, USA, 1994, *Nucl.Instr.&Meth.* **A355**(1995) 184.

[22] K.-J.Kim, P.Pierini, A.Sessler, V.Telnov, *LC95*, KEK, Japan, March 1995.

[23] V.Telnov, K.J.Kim, see *in Int.Linear Collider Tech.Review Committee Report*, SLAC-Rep-471 (1996).

[24] V.Telnov, *Proc.of Workshop 'Photon 95',* Sheffield, UK, April 1995.

[25] D.Miller, DESY-95-183, Sept.1995.

[26] D.Miller,*Proc.of Workshop on Phys. and Exper. with Linear Colliders,* Sept, 1995, Morioka-Appi, Japan, p.305.

[27] V.Telnov,*Proc.of Workshop on Phys. and Exper. with Linear Colliders,* Sept, 1995, Morioka-Appi, Japan, p.664.

[28] D.Schulte, e^+e^- *Collisions at TEV Energies: the Physics Potential, DESY 96-123D*, 1996, p.463.

[29] V.Telnov, *SLAC-PUB 7337*, SLAC, Oct.1996, submitted to Phys.Rev.Letters.

[30] *Proc.of Workshop on Gamma-Gamma Colliders*, Berkeley CA, USA, 1994, *Nucl. Instr. &Meth.* **A355**(1995)1–194.

[31] *Zeroth-Order Design Report for NLC*, SLAC-474, 1995.

[32] I.Ginzburg,*Proc. of IX Intern. Workshop on Photon-Photon collisions*, San Diego 1992, World Scientific.

[33] S.Brodsky, *Proc.of Workshop on Physics and Exper.with Linear* e^+e^- *Colliders*, Waikoloa, Hawaii, Apr.1993, World Scientific, 1993, p.295.

[34] M. Baillargeon, G. Belanger, and F. Boudjema, Proc. of the *"Two-Photon Physics from DAΦNE to LEP200 and Beyond"*, 2-4 February 1994, Paris, ENSLAPP-A-473-94, hep-ph/9405359.

[35] S.Brodsky, P.Zerwas, *Proc.of Workshop on Gamma-Gamma Colliders,* Berkeley CA, USA, 1994, *Nucl.Instr.&Meth.* **A355**(1995)19.

[36] M.Chanowitz, *Proc.of Workshop on Gamma-Gamma Colliders,* Berkeley CA, USA, 1994, *Nucl.Instr.&Meth.* **A355**(1995)42.

[37] I.Ginzburg, *Proc.of Workshop on Gamma-Gamma Colliders,* Berkeley CA, USA, 1994, *Nucl.Instr.&Meth.* **A355**(1995)63.

[38] I.Ginzburg, *Proc.of Workshop 'Photon 95',* Sheffield, UK, April 1995,

[39] e^+e^- *Collisions at 500 GeV*, Preprint *DESY 93–123C* (1993).

[40] *Proc. of the 2nd Workshop on "Physics and Experiments with Linear* e^+e^- *Colliders"*, eds. F. Harris, S. Olsen, S. Pakvasa and X. Tata, Waikoloa (1993) World Scientific Publishing, Singapore.

[41] *Photon '95 (1995)*, Eds. D. Miller et al., World Sc. Singapore

[42] e^+e^- *Collisions at TeV Energies*, Preprint *DESY 96–123D* (1996).

[43] I.F. Ginzburg, *Proc. 9th International Workshop on Photon – Photon Collisions*, San Diego (1992) World Sc. Singapore, 474 –501.

[44] S. Brodsky and P. Zerwas, *Nucl. Instr. &Meth.* **A355** (1995) 19.

[45] I.F. Ginzburg, in ref [42], 455.

[46] *Zeroth-order Design Report for the NLC, SLAC Report*, (1996), p.474.

[47] G.L. Kotkin and V.G. Serbo, Preprint *hep-ph/9611345* (1996).

[48] T. Barklow, *Proceedings of the 1990 DPF Summer Study on High-Energy Physics: "Research Directions for the Decade"*, Editor E. Berger, Snowmass, CO, June 25 - July 13, 1990, p. 440.

[49] J.F. Gunion and H.E. Haber, *Proceedings of the 1990 DPF Summer Study on High-Energy Physics: "Research Directions for the Decade"*, Editor E. Berger, Snowmass, CO, June 25 - July 13, 1990, p. 206, *Phys. Rev.* **D48** (1993) 5109.

[50] V.E. Balakin, I.F. Ginzburg, In ref. [40], 605.

[51] I. Watanabe, Proceedings of the INS Workshop on the Physics of e^+e^- and $\gamma\gamma$ Collisions at Linear Accelerators, Tokyo, Japan, 20-22 December, 1994, p. 139, hep-ph/9504226.

[52] J.F. Gunion, P.C. Martin, Report UCD-96-15, July 1996, hep-ph/9607360; Report UCD-96-34, October 1996, hep-ph/9610417, to be published in the *Proceedings of 1996 DPF/DPB Summer Study on New Directions for High-energy Physics* (Snowmass 96), Snowmass, CO, 25 June – 12 July 1996.

[53] D.L. Borden, D.A. Bauer, D.O. Caldwell, Phys. Rev. **D48** (1993) 4018.

[54] O.J.P. Éboli, M.C. Gonzalez-Garcia, F. Halzen, and D. Zeppenfeld, *Phys. Rev.* **D48** (1993) 1430.

[55] M. Baillargeon, G. Belanger and F. Boudjema, *Phys. Rev.* **D51** (1995) 4712.

[56] G. Jikia, A. Tkabladze, Proc. of the *Workshop on gamma–gamma colliders*, March 28-31, 1994, Lawrence Berkeley Laboratory, *Nucl. Instr. & Meth.* **A355** (1995) 81; *Phys. Rev.* **D54** (1996) 2030;

[57] D. L. Borden, V. A. Khoze, W. J. Stirling, and J. Ohnemus, *Phys. Rev.* **D50** (1994) 4499; V. Khoze, in ref.[41], p. 392.

[58] A. Bartl et al., Report LBL-39413, November 1996, to be published in the *Proceedings of 1996 DPF/DPB Summer Study on New Directions for High-Energy Physics* (Snowmass 96), Snowmass, CO, 25 June - 12 July 1996.

[59] G.L. Kane, G.D. Kribs, S.P. Martin and J.D. Wells, *Phys. Rev.* **D53** (1996) 213.

[60] G. Jikia, Phys.Lett. **B298** (1993) 224; ref. [40], p. 558; *Nucl. Phys.* **B405** (1993) 24.

[61] M.S. Berger *Phys. Rev.* **D48** (1993) 5121.

[62] D.A. Dicus and C. Kao, *Phys. Rev.* **D49** (1994) 1265.

[63] D.A. Morris, T.N. Truong, D. Zappala, Phys. Lett. **B323** (1994) 421.

[64] E.E. Boos, I.F. Ginzburg, K.V. Melnikov, T. Sack, S.A. Shichanin, Zeitschr. Phys. C 56 (1992) 487.

[65] I.F. Ginzburg, Preprint TP 28 (182) Inst. of Mathem. Novosibirsk (1990).

[66] G.J. Gounaris and F.M. Renard, *Z. Phys.* **C69** (1996) 513.

[67] I.F. Ginzburg, I.P. Ivanov. In preparation.

[68] B. Grzadkowski and J.F. Gunion, *Phys. Lett.* **B294**, 261 (1992).

[69] J.F. Gunion and J. Kelly, *Phys. Lett.* **B333** (1994) 110.

[70] M. Krämer, J. Kün, M.I. Stong and P.M. Zerwas, *Z. Phys.* **C64** (1994) 21.

[71] S. Weinberg, *Phys. Rev.* **D42** (1990) 860.

[72] J.F. Gunion, A. Stange, S. Willenbrock, Report UCD-95-28, December 1995, hep-ph/9602238.

[73] I.F. Ginzburg, G.L. Kotkin, V.G. Serbo, V.I. Telnov, Sov. ZhETF Pis'ma. 34 (1981) 514; *Nucl. Instr. &Meth.A*) 205 (1983) 47; I.F. Ginzburg, G.L. Kotkin, S.L. Panfil, V.G. Serbo, V.I. Telnov, *Nucl. Instr. &Meth.A* 219 (1983) 5.

[74] I.F. Ginzburg, G.L. Kotkin, S.L. Panfil, V.G. Serbo, Nucl. Phys. **B228** (1983) 285, E.: **B243** (1984) 550.

[75] S.Y.Choi, F.Shrempp, Phys.Lett. **B272** (1991) 149; E.Yehudai, Phys. Rev. **D44** (1991) 3434; A.Miyamoto in Proc. 2-nd Workshop on JLC, KEK 91-10 (1991).

[76] G. Bélanger and F. Boudjema, *Phys. Lett.* **B288** (1992) 210.

[77] M. Baillargeon and F. Boudjema *Phys. Lett.* **B317** (1993) 371.

[78] F.T. Brandt, O.J.P. Éboli, E.M. Gregores, M.B. Magro, P.G. Mercadante and S.F. Novaes, *Phys. Rev.* **D50** (1994) 5591.

[79] M. Baillargeon, G. Bélanger, F. Boudjema and G. Jikia, Proceedings of the 3rd Workshop e^+e^- *Collisions at TeV Energies: the Physics Potential, Part D*, DESY, Hamburg, Germany, August 30 – September 1, 1995, p. 511.

[80] F. Boudjema, in Physics and Experiments with Linear e^+e^- Colliders, Waikoloa, Hawaii, 1993, Ed. F.A. Harris *et al.*, World Sci., vol. II, p. 712; F. Boudjema, in Physics and Experiments with Linear e^+e^- Colliders, Morioka, Japan, September 8–12, 1995.

[81] A. Denner, S. Dittmaier, and R. Schuster, *Nucl. Phys.* **B452** (1995) 80; Proceedings of the 3rd Workshop e^+e^- *Collisions at TeV Energies: the Physics Potential, Part D*, DESY, Hamburg, Germany, August 30 – September 1, 1995, p. 233; Report BI-TP 96/03, WUE-ITP-96-001, hep-ph/9601355.

[82] G. Jikia, Proceedings of the Workshop Physics and Experiments with Linear e^+e^- Colliders, Morioka, Japan, September 8–12, 1995; Report FREIBURG-THEP-96-23, December 1996, hep-ph/9612380.

[83] A.Denner, S. Dittmaier, *Nucl. Phys.* **B398** (1993) 239; *DESY–93–123C* (1993) 171; M. Böhm, S. Dittmaier, *Nucl. Phys. B409* (1993) 3.

[84] I.F. Ginzburg, Sov.Yad.Fiz. (Phys. At. Nucl.) **58** (1995) 326.

[85] F. Boudjema et al., *DESY 96–123D* (1996) 225.

[86] I.F. Ginzburg, V.A. Ilyin, A.E. Pukhov, V.G. Serbo, S.A. Shichanin, Phys. At. Nucl. **56** (1993) 39.

[87] G. Jikia, A. Tkabladze, *Phys. Lett.* **B323** (1994) 453.

[88] G. Jikia, A. Tkabladze, *Phys. Lett.* **B332** (1994) 441.

[89] G. Jikia, Proc. of the *Workshop on gamma–gamma colliders*, March 28-31, 1994, Lawrence Berkeley Laboratory, *Nucl. Instr. & Meth.* **A355** (1995) 84; *Nucl. Phys.* **B437** (1995) 520.

[90] K. Cheung, *Phys. Lett.* **B323** (1994) 85; *Phys. Rev.* **D50** (1994) 4290.

[91] I.F. Ginzburg, V.A. Ilyin, A.E. Pukhov, V.G. Serbo, In preparation.

[92] I.F. Ginzburg, V.A. Ilyin, In preparation.

[93] I.I. Bigi, F. Gabbiani, V.A. Khoze, *Nucl. Phys.* **B406** (1993) 3.

[94] V.S. Fadin, V.A. Khoze, M.I. Kotskii *Z. Phys.* **C64** (1994) 45.

[95] V. Fadin, V. Khoze, JETP Lett. **46** (1987) 585; Sov. J.Nucl. Phys. **48** (1988) 309.

[96] H. Murayama and W.B. Kilgore, Proc. of the *Workshop on gamma–gamma colliders*, March 28-31, 1994, Lawrence Berkeley Laboratory.

[97] I.F. Ginzburg, in ref. [30], p. 63.

[98] *Tests of alternative models at a 500 GeV NLC*, ed. F.Boudjema & F.M.Renard. *ENSLAPP–A–365/92* (1992).

[99] F. Cuypers, G.J.van Oldenborgh, R. Rückl, Nucl.Phys. **B383** (1992) 45; **409** (1993) 128, 144; F. Cuypers, Phys.Rev **D49** (1994) 3075.

[100] I.F. Ginzburg, D.Yu. Ivanov, Phys. Lett. **276B** (1992) 214; A. Beliaev, E. Boos, A. Pukhov, Phys. Lett. **B296** (1992) 452; F. Boudjema in ref.[98].

[101] J.E. Cieza Montalvo, O.J.P. Eboli, Phys. Rev. **D47** (1993) 837; O.J.P. Eboli, E.M. Gregores et al., Phys. Lett. **311B** (1993) 471.

[102] I.F. Ginzburg, S.L. Panfil, Sov. J. Nucl. Phys. **36** (1982) 850.

[103] S.I. Polityko, Sov. Yad. Fiz. **43** (1986)146; **56** (1993) 144.

[104] I.F. Ginzburg, G.L. Kotkin, S.I. Polityko, Sov. Yad. Fiz. **37** (1983) 368; **40** (1984) 1495; Phys. At. Nucl.**56** (1993) 1487.

[105] R. Engel et al. in ref. [42], 483.

[106] Pisin Chen, T. Barklow, M. Peskin, Phys. Rev. **D49** (1994) 3209.

[107] Budnev V.M., I.F.Ginzburg, G.V.Meledin & V.G.Serbo, Phys.Rep.**15C** (1975) 181.

[108] I.F. Ginzburg, D.Yu. Ivanov, Phys.Rev. **D54** (1996) 5523–5535.

[109] I.F. Ginzburg, S.L. Panfil and V.G. Serbo, Nucl.Phys. **B284** (1987) 685; **B296** (1988) 569.

[110] I.F. Ginzburg and D.Yu. Ivanov, Nucl. Phys. B (Proc. Suppl.) 25B (1992) 224; Nucl.Phys. B388 (1992) 376.

[111] A.D.Mueller Nucl. Phys. **B415** (1994) 373.

[112] D.Yu. Ivanov, Phys.Rev. **D53** (1996) 3564.

[113] D.J. Miller, A. Vogt in ref. [42], 473.

[114] F.R.Arutyunian and V.A.Tumanian,*Phys.Lett.* **4** (1963)176; R. H. Milburn, *Phys. Rev. Lett.* **10** (1963)75.

[115] L.Landau,E.Lifshits, *Kvantovaya mekhanika*, v.**1**, M.Nauka.

[116] M.Xie, K-J.Kim, A.Sessler, *Proc.of Workshop on Gamma-Gamma Colliders,* Berkeley CA, USA, 1994, *Nucl.Instr.&Meth.* **A355**(1995)163.

[117] R.Palmer, SLAC-PUB 4707(1988).

[118] V.Telnov, *CLIC Note 311* , CERN, June 1996.

[119] T.Takahashi, K.Yokoya, V.Telnov, M.Xie and K.Kim, Proc. of Snowmass Workshop, July 1996.

[120] P.Chen, T.Ohgaki, A.Spitkovsky, T.Takahashi, K.Yokoya, in preparation

[121] C.Travier, *Nucl.Instr.&Meth.* **A340**(1994)26.

[122] G.Silvestrov, V.Telnov, Proc. of LC95, KEK, March 1995

[123] Y.Yasui, I.Watanabe, J.Kodaira and I.Endo,
Nucl. Instr. &Meth. **A335**(1993)385.

[124] V.Telnov, to be published.

[125] M.Battaglia, V.Telnov, to be published.

[126] G.Schuler, T.Sjostrand, CERN-TH/96-119, May 1996.

[127] B.Stuart et al., UCLA-JC-120,225.

[128] For a review, see M. Perry and G. Mourou, *Science*, **264** (1994)917.

[129] D.Strickland and G.Mourou, *Opt.Commun.* **56** (1985) 219.

[130] C.Bamber et al., *Opt.Lett.* submitted (1995)

[131] D.Meyerhofer, *Proc.of Workshop on Gamma-Gamma Colliders,* Berkeley CA, USA, 1994, *Nucl. Instr. &Meth.* **A355**(1995)113.

[132] C.Clayton, N.Kurnit, D.Meyerhofer, *Proc.of Workshop on Gamma-Gamma Colliders,* Berkeley CA, USA, 1994, *Nucl. Instr. &Meth.* **A355**(1995)121.

[133] E.L. Saldin, V.P. Sarantsev, E.A. Schneidmiller and M.V. Yurkov, *Proc.of the Second Workshop "Physics at VLEPP"*, Protvino, Russia, 1992, Vol. 2. p. 96, in Russian.

[134] E.L. Saldin, V.P. Sarantsev, E.A. Schneidmiller and M.V. Yurkov, *Proc.of the XIII Conf. on Charged Particle Accelerators*, Dubna, Russia, 1992, Vol. 1. p. 36, in Russian.

[135] E.L. Saldin, V.P. Sarantsev, E.A. Schneidmiller and M.V. Yurkov, Preprint *JINR E9-94-70*, Dubna, 1994.

[136] E.L. Saldin, V.P. Sarantsev, E.A. Schneidmiller and M.V. Yurkov, *Nucl. Instr. &Meth.* **A339**(1994)583.

[137] V.A. Alexandrov, V.E. Balakin, E.A. Kushnirenko, A.A. Sery, N.A. Solyak and M.V. Yurkov, *Photon linear collider* 100×100 *GeV based on the VLEPP physics and technology, Proc. LC 93 Workshop*, SLAC, Stanford, October, 1993.

[138] E.L. Saldin, V.P. Sarantsev, E.A. Schneidmiller, Yu.N. Ulyanov and M.V. Yurkov, Preprint *DESY 94-243*, DESY, Hamburg, 1994.

[139] E.L. Saldin, V.P. Sarantsev, E.A. Schneidmiller, Yu.N. Ulyanov and M.V. Yurkov, *Nucl. Instr. &Meth.* **A361**(1995)101.

[140] E.L. Saldin, V.P. Sarantsev, E.A. Schneidmiller, Yu.N. Ulyanov and M.V. Yurkov, *Proc.of the Sixth International Workshop on Linear Colliders LC95*, KEK Proceedings 95-5, Tsukuba, Japan, August 1995, Vol. III, p.1919.

[141] S. Hiramatsu, S. Hashimoto and Y. Ishida, *Nucl. Instr. &Meth.* **A355** (1995) 133.

[142] R. Corsini and A. Mikhailichenko, *Proc.of the Sixth International Workshop on Linear Colliders LC95*, KEK Proceedings 95-5, Tsukuba, Japan, August 1995, Vol. III.

[143] K.-J. Kim, M. Xie and A.M. Sessler, *Nucl. Instr. &Meth.A* **A375**(1996)523.

[144] *Zeroth-Order Design Report for the Next Linear Collider*, Appendix B, *LBNL-PUB-5424*, SLAC Report 474, UCRL-ID-124161 (May 1996).

[145] E.L. Saldin, V.P. Sarantsev, E.A. Schneidmiller, Yu.N. Ulyanov and M.V. Yurkov, Preprint *JINR E9-94-237*, Dubna, 1994.